JOURNAL OF PETROLOGY | VOLUME 44 | NUMBER 11 | PAGES 2003–2032 | 2003 | DOI: 10.1093/petrology/egg068

Relationships between Mafic and Peralkaline Silicic Magmatism in Continental Rift Settings: a Petrological, Geochemical and Isotopic Study of the Gedemsa Volcano, Central Ethiopian Rift

A. PECCERILLO[1]*, M. R. BARBERIO[1], G. YIRGU[2], D. AYALEW[2], M. BARBIERI[3] AND T. W. WU[4]

[1]DIPARTIMENTO DI SCIENZE DELLA TERRA, UNIVERSITY OF PERUGIA, PIAZZA UNIVERSITÀ, 06100, PERUGIA, ITALY

[2]DEPARTMENT OF GEOLOGY AND GEOPHYSICS, ADDIS ABABA UNIVERSITY, PO BOX 1176, ADDIS ABABA, ETHIOPIA

[3]DIPARTIMENTO DI SCIENZE DELLA TERRA, UNIVERSITY OF ROME 'LA SAPIENZA', ROME, ITALY

[4]DEPARTMENT OF GEOLOGY, UNIVERSITY OF WESTERN ONTARIO, LONDON, ONTARIO N6A 5B7, CANADA

RECEIVED SEPTEMBER 9, 2002; ACCEPTED MAY 9, 2003

Petrological and geochemical data are reported for basalts and silicic peralkaline rocks from the Quaternary Gedemsa volcano, northern Ethiopian rift, with the aim of discussing the petrogenesis of peralkaline magmas and the significance of the Daly Gap occurring at local and regional scales. Incompatible element vs incompatible element diagrams display smooth positive trends; the isotope ratios of the silicic rocks ($^{87}Sr/^{86}Sr$ = 0·70406–0·70719; $^{143}Nd/^{144}Nd$ = 0·51274–0·51279) encompass those of the mafic rocks. These data suggest a genetic link between rhyolites and basalts, but are not definitive in establishing whether silicic rocks are related to basalts through fractional crystallization or partial melting. Geochemical modelling of incompatible vs compatible elements excludes the possibility that peralkaline rhyolites are generated by melting of basaltic rocks, and indicates a derivation by fractional crystallization plus moderate assimilation of wall rocks (AFC) starting from trachytes; the latter have exceedingly low contents of compatible elements, which precludes a derivation by basalt melting. Continuous AFC from basalt to rhyolite, with small rates of crustal assimilation, best explains the geochemical data. This process generated a zoned magma chamber whose silicic upper part acted as a density filter for mafic magmas and was preferentially tapped; mafic magmas, ponding at the bottom, were erupted only during post-caldera stages, intensively mingled with silicic melts. The large number of caldera depressions found in the northern Ethiopian rift and their coincidence with zones of positive gravity anomalies suggest the occurrence of numerous magma chambers where evolutionary processes generated silicic peralkaline melts starting from mafic parental magmas. This suggests that the petrological and volcanological model proposed for Gedemsa may have regional significance, thus furnishing an explanation for the large-volume peralkaline ignimbrites in the Ethiopian rift.

KEY WORDS: *peralkaline rhyolites; geochemistry; Daly Gap; Gedemsa volcano; Ethiopian rift*

INTRODUCTION

Regions of continental break-up are often associated with extensive magmatic activity (e.g. White & McKenzie, 1989). This commonly consists of huge volumes of flood basalts and variable amounts of silicic volcanics, forming the so-called Large Igneous Provinces (LIPs). In most cases a wide silica gap occurs

*Corresponding author. Telephone: +39 (075) 5852608. Fax: +39 (075) 5852603. E-mail: pecceang@unipg.it

between silicic and mafic compositions (Daly Gap), with small amounts or an absence of intermediate rocks (e.g. Bellieni *et al*., 1985; Garland *et al*., 1995).

A widely accepted model of continental break-up and associated large-scale mafic magmatism is that these are related to the upwelling of mantle plumes from the deep mantle which impinge on the base of the lithosphere (e.g. White & McKenzie, 1989; Campbell & Griffiths, 1992; Davies, 1998; Rogers *et al*., 2000; Macdonald *et al*., 2001). Mafic magmas result from mantle melting, with variable contributions from plume, asthenosphere and lithosphere (e.g. Marty *et al*., 1996; Pik *et al*., 1999). However, the genesis of the associated silicic magmas and the nature of the Daly Gap remain major problems in igneous petrology (e.g. Lightfoot *et al*., 1987; Bonnefoi *et al*., 1999).

The Ethiopian rift valley is a major zone of continental break-up and is the site of extensive magmatic activity, which gave rise to a large Oligocene to Miocene plateau and widespread Plio-Quaternary volcanism in Afar and along the rift (e.g. Merla *et al*., 1979; Mohr & Zanettin, 1988). Both plateau and rift volcanism include a bimodal distribution of mafic and silicic rocks. Weakly alkaline silicic rocks are present in the plateau series, whereas large ignimbritic sheets and plinian pumice fallout deposits with a peralkaline rhyolitic composition cover the rift floor and a large part of the surrounding areas (e.g. Yemane *et al*., 1999). Therefore, peralkaline silicic magmatism is an important geological feature of the Ethiopian province. Understanding it has significance for several first-order geological issues, including conditions of continental break-up and rift opening, mechanisms of magma emplacement and evolution, and construction of crust in the rift environments.

Most studies on Ethiopian rift magmatism have been carried out at a regional scale (e.g. Hart *et al*., 1989; Trua *et al*., 1998; Ayalew *et al*., 1999; Yemane *et al*., 1999), and detailed investigations on single volcanoes are scarce. In this paper, we report on a petrological and geochemical study of Gedemsa, a silicic peralkaline volcano containing minor basaltic scoriae and lavas, which is located along the axis of the central Ethiopian rift (Fig. 1). Compositional data on whole rocks and minerals are discussed with the aim of placing constraints on the genesis of the silicic magmas and on possible models of the volcano plumbing system, both at Gedemsa and along the Ethiopian rift.

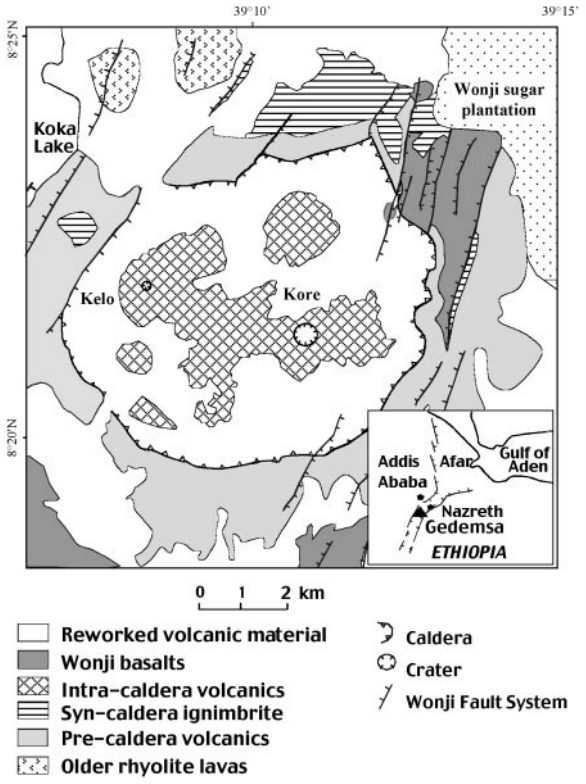

Fig. 1. Schematic geological map of the Gedemsa volcano.

GEOLOGICAL AND VOLCANOLOGICAL BACKGROUND

Volcanism in Ethiopia has occurred from Oligocene to Present (e.g. Merla *et al*., 1979; Kazmin *et al*., 1980; Berhe *et al*., 1987; Mohr & Zanettin, 1988). It has built up a thick succession of lavas and pyroclastic rocks, typically 500–1500 m thick, which covers an area of about 6×10^5 km^2, and at present forms the western and eastern uplifted plateau and the Ethiopian rift and Afar. The volcanic sequence rests either directly on Precambrian basement or on Mesozoic sedimentary sequences.

The volcanic activity was associated with various stages of rift formation, including the Red Sea, Gulf of Aden, Afar and Main Ethiopian Rift. Its evolution is very complex, but consists of three main stages. During the first stage (about 50–10 Ma), the Ethiopian plateau was constructed by eruptions of flood tholeiitic to transitional basalt lava flows, and interbedded mildly alkaline trachytic and rhyolitic ignimbrites (e.g. Mohr & Zanettin, 1988). Apparently, most of the plateau lavas were erupted over a relatively short period of time, around 30 ± 1 Ma (Hofmann *et al*., 1997). A second stage of activity occurred around 10–5 Ma and constructed several shield volcanoes made of transitional to Na-alkaline basalts and minor trachytes (e.g. Piccirillo *et al*., 1979). The final stage is Pliocene to Present and is more directly related to formation of

the Ethiopian rift and Afar. In the Main Ethiopian Rift, recent volcanism consists of rhyolitic and trachytic pyroclastic rocks and minor lavas, and of volumetrically subordinate basalts. Intermediate rocks are rare. Silicic rocks either form large central volcanoes with summit calderas (e.g. Gedemsa, Fantale and Gebre Gebade), or occur as large, low-aspect ratio, ignimbrites and plinian pumice fallout covering the rift floor. Di Paola (1972) suggested that most ignimbrites have been erupted from distension fractures related to rift opening, but in some cases (e.g. at Fantale) a provenance from central volcanoes is evident.

Basalts mostly form cinder cones, small lava flows, and some tuff rings, tuff cones and maars, mostly aligned in a NE–SW direction along the rift-related faults of the Wonji Fault Belt (Wonji Basalts; Mohr, 1967). Basalt eruptions also occurred on the plateau areas during Quaternary time, as best exemplified by the Lake Tana fissural basalt field. Some Plio-Quaternary trachytic to phonolitic volcanoes (Zuquala, Whachacha and Yerer) occur along the margins of the rift (Gasparon *et al.*, 1993).

The Gedemsa volcano is located in the central Ethiopian rift, about 100 km SE of Addis Ababa, near the town of Nazreth (Fig. 1). The volcano has a maximum elevation of about 300 m above the rift floor, and is characterized by a large central caldera about 8 km in diameter, extensively cut by the Wonji fault system (Thrall, 1973). The pre-caldera suite is formed by lava domes and flows, and plinian pumice fallout deposits. Ignimbrites represent the main syn-caldera rocks. Field evidence suggests that caldera formation is not related to a single large-scale explosive event, but rather to several moderate-volume pyroclastic eruptions, which took place in different sectors of the volcano (Cioni *et al.*, 2001). The post-caldera rocks form several small coalescing cones mostly located inside the caldera depression. These consist of obsidian domes and flows and of pyroclastic deposits, mainly fall pumices. Notably, the intra-caldera products contain inclusions of mafic–intermediate material in the host silicic magma. Mingling between mafic and silicic magmas is also observed, but to a much smaller degree, in the juvenile components of syn-caldera ignimbrites.

The final activity took place along a fault of the Wonji system, which cuts the eastern border of the volcano (Fig. 1). This is not directly related to Gedemsa, as it is a part of the younger volcanism forming rows of basaltic centres at a regional scale along the Wonji Fault Belt. In the Gedemsa area the Wonji Basalts form two small eruptive centres, one sited inside the caldera near the northeastern margin, and one occurring at the base of the northeastern flank of the Gedemsa volcano. Although these late basaltic eruptions are not structurally related to Gedemsa, lavas and scoriae occurring inside the caldera show evidence of mingling with salic magma.

Table 1: K/Ar ages of alkali feldspar separated from a pre-caldera obsidian (GD4) and from a post-caldera lava (GD7)

Sample	$^{40}Ar_{rad}$ (nl/g)	K (%)	$^{40}Ar_{air}$ (%)	Age (Ma)
GD4	0·0614	5·055	86·70	0·319 ± 0·02
GD7	0·0458	4·528	86·68	0·265 ± 0·02

K concentration determined by inductively coupled plasma mass spectrometry.

New K/Ar ages have been determined at the Geochron Laboratories, Cambridge, USA, on separated sanidine–anorthoclase phenocrysts from a pre-caldera obsidian (GD4, NE caldera escarpment) and from a post-caldera rhyolite lava (GD7, Kore crater rim). Duplicate analyses gave ages of 0·32 ± 0·02 ka for pre-caldera and 0·26 ± 0·02 ka for post-caldera activity (Table 1).

SAMPLING, PETROGRAPHY AND MINERAL CHEMISTRY

Our sampling attempted to encompass the entire eruptive sequence of Gedemsa. Pre- and syn-caldera rocks come predominantly from the northeastern escarpment of the caldera, where these rocks are best exposed. Here, the pre-caldera sequence consists of obsidian lavas, and a thick deposit of pumice fallout; a high-aspect-ratio ignimbrite marks the transition from pre- to post-caldera phases. The post-caldera samples were collected mainly from domes, flows and pyroclastic deposits inside the caldera. Basaltic scoria and lava samples along the Wonji fault were collected from the intra-caldera and lateral centres. Several mafic–intermediate enclaves occurring within the post-caldera rocks have also been studied. Basic petrographical studies have been carried out on approximately 150 samples from various stratigraphic levels. Mineral compositions have been determined on selected samples (Table 2 and Fig. 2).

Based on the TAS classification diagram (Le Bas *et al.*, 1986), most of the samples are rhyolites and trachytes, whereas mafic rocks are typical transitional basalts. The inclusions in post-caldera lavas range in composition from basalt to benmoreite (Table 3).

Basalts

The intra-caldera basaltic activity along the Wonji fault (Wonji Basalts) formed surge deposits, followed

Table 2: Representative electron microprobe analyses of minerals from Gedemsa rocks

	Olivine												
Rock type:	Basalt		Basalt		Enclave		Enclave		Pre-caldera trachyte	Post-caldera rhyolite		Ignimbrite	
Sample:	GD65		GD64		GD13		GD10		GD4	GD81		GD26	
	ph-core	ph-rim	ph-core	ph-rim	ph-core	ph-rim	ph-core	ph-rim	ph-core	ph-core	ph-rim	ph-core	ph-rim
SiO_2	40·15	38·38	41·24	40·01	39·76	38·22	38·54	35·29	29·79	39·56	34·16	30·33	30·03
TiO_2	—	0·07	0·02	—	0·02	0·13	—	0·06	—	0·04	0·02	0·06	0·09
Al_2O_3	0·09	0·16	—	—	0·02	0·05	0·03	0·03	—	0·03	—	—	—
Cr_2O_3	0·03	—	—	—	—	—	0·01	0·07	—	—	—	—	0·03
Fe_2O_3	—	—	0·03	0·70	0·08	—	0·09	—	1·40	0·35	0·48	—	0·19
FeO	16·92	23·59	10·31	14·27	19·21	22·37	25·12	41·66	63·54	18·74	44·48	65·27	65·52
MnO	0·20	0·46	0·31	0·27	0·20	0·40	0·46	1·14	6·36	0·29	1·72	4·99	5·14
NiO	0·09	0·13	0·06	0·02	0·04	—	—	—	—	—	—	—	—
MgO	43·77	37·29	49·22	45·58	42·30	37·65	37·18	22·73	0·08	42·37	19·92	0·24	0·43
CaO	0·20	0·30	0·20	0·14	0·25	0·26	0·29	0·22	0·58	0·23	0·17	0·52	0·46
Sum	101·45	100·38	101·39	100·99	101·88	99·08	101·72	101·20	101·75	101·62	100·95	101·41	101·89
Fo	81·78	73·12	88·94	84·11	79·20	74·39	71·79	48·46	0·20	79·36	43·10	0·59	1·06
Fa	17·74	25·95	10·48	15·42	20·25	24·79	27·30	49·82	89·98	20·03	54·52	91·51	90·92

	Clinopyroxene													
Rock type:	Basalt		Enclave		Enclave		Pre-caldera trachyte		Post-caldera rhyolite		Post-caldera rhyolite		Ignimbrite	
Sample:	GD64		GD10		GD15		GD4		GD81		GD12		GD26	
	ph-core	ph-rim	mph	mph	mph	grms	ph-core	ph-rim	ph-core	ph-rim	ph-core	ph-rim	ph-core	ph-rim
SiO_2	49·83	49·25	48·45	48·71	51·22	48·53	47·36	47·47	48·64	49·78	48·95	49·08	47·36	48·24
TiO_2	1·55	1·64	1·93	1·94	1·01	2·20	0·48	0·50	0·45	0·47	1·20	1·23	1·05	4·35
Al_2O_3	4·82	4·91	4·04	4·05	2·40	4·73	0·20	0·15	0·19	0·16	0·64	0·56	0·55	0·53
Cr_2O_3	0·33	0·36	0·02	0·04	0·05	—	—	—	0·02	—	0·02	—	—	0·02
Fe_2O_3	1·53	2·46	3·43	2·97	2·27	2·56	3·91	3·44	3·33	6·33	16·99	16·99	2·41	13·70
FeO	6·72	6·21	7·74	9·65	9·24	9·23	26·83	27·18	27·04	21·66	20·58	20·14	26·89	18·70
MnO	0·17	0·20	0·41	0·59	0·79	0·64	2·17	2·29	1·64	1·20	1·04	1·10	2·63	1·72
NiO	—	—	—	—	—	—	—	—	—	—	—	—	—	—
MgO	14·27	14·19	13·25	12·62	15·22	13·33	0·13	0·14	0·90	2·33	0·30	0·23	0·41	1·01
CaO	20·99	21·32	19·49	19·13	18·09	18·99	18·72	18·94	17·28	15·19	3·67	3·11	19·19	3·91
Na_2O	0·38	0·29	0·63	0·59	0·39	0·44	0·81	0·69	1·30	2·89	6·10	6·41	0·57	6·63
K_2O	—	—	—	—	—	—	0·02	—	0·03	0·02	1·46	1·45	0·02	1·18
Sum	100·58	100·83	99·39	100·29	100·68	100·65	100·63	100·79	100·82	100·02	100·95	100·30	101·08	99·99
En	41·98	41·31	39·47	37·54	43·49	39·43	0·41	0·44	2·89	7·96	1·27	1·00	1·28	4·55
Fe	13·64	14·08	18·79	21·56	19·36	20·21	57·34	57·07	57·18	54·74	87·58	89·27	55·62	82·80
Wo	44·38	44·61	41·73	40·90	37·15	40·37	42·25	42·49	39·93	37·30	11·15	9·73	43·10	12·66
Mg no.	0·76	0·75	0·68	0·64	0·69	0·66	0·01	0·01	0·05	0·13	0·01	0·01	0·02	0·05

	Plagioclase							
Rock type:	Basalt		Basalt		Enclave		Enclave	
Sample:	GD64		GD65		GD83f		GD13	
	ph-core	ph-rim	ph-core	ph-rim	ph-core	ph-rim	ph-core	ph-rim
SiO_2	47·97	55·93	53·60	50·71	66·37	65·32	47·48	53·11
TiO_2	0·04	0·10	—	0·06	0·05	0·09	0·04	0·12
Al_2O_3	33·24	28·13	29·63	31·31	20·30	21·40	33·51	29·23
Fe_2O_3	0·54	0·79	0·50	0·59	0·73	0·18	0·58	0·71
MgO	0·06	0·04	0·07	0·09	0·16	0·02	0·14	0·17
CaO	16·29	10·12	12·20	14·60	2·76	2·38	16·32	11·84
Na_2O	2·26	5·49	4·41	2·98	7·28	8·56	1·99	4·04
K_2O	0·08	0·33	0·49	0·12	2·80	2·38	0·05	0·20
SrO	—	—	—	—	—	—	—	—
BaO	—	—	—	—	—	—	—	—
Sum	100·48	100·93	100·90	100·46	100·45	100·33	100·11	99·42
Ab	19·97	48·59	38·43	26·78	68·37	74·82	18·02	37·71
An	79·56	49·49	58·76	72·51	14·32	11·50	81·68	61·07
Or	0·47	1·92	2·81	0·71	17·30	13·69	0·30	1·23

	Anorthoclase					Sanidine	
Rock type:	Pre-caldera trachyte		Post-caldera rhyolite		Ignimbrite	Post-caldera rhyolite	
Sample:	GD4		GD81		GD26	GD12	
	ph-core	ph-rim	ph-core	ph-rim	mph	ph-core	ph-rim
SiO_2	66·85	66·85	67·91	66·95	64·58	65·64	64·92
TiO_2	0·08	0·07	0·02	0·01	0·10	0·04	0·07
Al_2O_3	18·58	18·67	18·97	17·34	20·65	22·14	21·89
Fe_2O_3	0·42	0·31	0·76	2·26	0·30	0·30	0·29
CaO	0·11	0·13	0·05	0·02	1·15	2·07	2·23
Na_2O	7·16	7·21	7·04	6·67	6·55	8·25	8·20
K_2O	5·98	5·70	5·66	6·74	3·83	1·71	2·14
SrO	0·02	0·03	—	—	0·05	—	—
BaO	0·06	0·18	—	—	2·54	—	—
Sum	99·29	99·15	100·41	100·04	99·75	100·04	100·41
Ab	64·18	65·35	65·23	60·00	67·49	60·00	65·23
An	0·54	0·65	0·26	0·10	6·55	0·10	0·26
Or	35·27	34·00	34·51	39·90	25·97	39·90	34·51

by a cinder cone and a small aa lava flow. Surge deposits consist of indurated layers of coarse ash, lapilli and scoriae, plastering the northeastern border of the caldera; juvenile material displays variable composition, with evidence of mingling between salic and mafic magma, especially at the base of the deposit (Cioni *et al.*, 2001). Lavas and strombolian scoriae are poorly to moderately porphyritic [porphyritic index (P.I.) = 5–20], with dominant zoned phenocrysts of olivine (Fo_{89-73}), diopsidic clinopyroxene, and minor

Table 2: continued

	Magnetite	Ilmenite		Aenigmatite
Rock type:	Basalt	Basalt		Post-caldera rhyolite
Sample:	GD65	GD3		GD12
	grms	grms		mph
SiO_2	0·20	—	SiO_2	40·99
TiO_2	19·81	9·63	TiO_2	8·76
Al_2O_3	3·12	2·09	Al_2O_3	0·38
Cr_2O_3	0·47	0·71	Cr_2O_3	—
Fe_2O_3	26·24	46·60	Fe_2O_3	41·00
FeO	43·76	37·59	FeO	1·11
MnO	0·47	0·33	MnO	0·12
NiO	—	—	CaO	0·29
MgO	3·20	1·13	Na_2O	7·08
CaO	0·31	0·12	K_2O	0·01
Sum	97·58	98·20	Sum	99·73

ph, phenocryst; mph, microphenocryst; grms, groundmass; —, not detected; Mg no. = $Mg/(Mg + Fe^{2+})$.

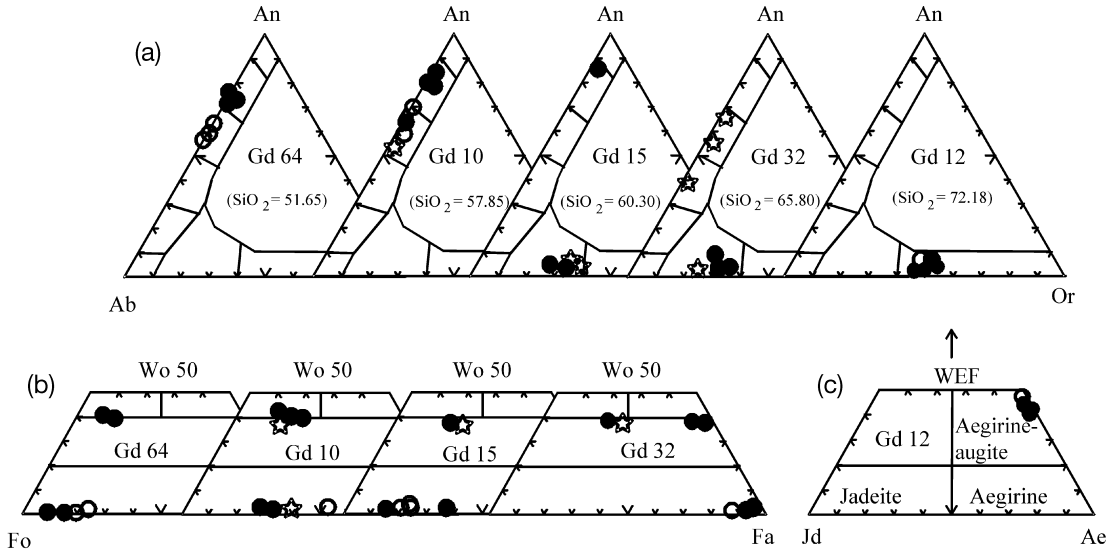

Fig. 2. Representative compositions of feldspars (a), clinopyroxene and olivine (b), and alkali pyroxene (c) in the Gedemsa rocks. ●, phenocryst core; ○, phenocryst rim; open stars, groundmass. SiO_2 content of host rocks is reported in parentheses in (a).

plagioclase ($An_{80–50}$), set in a groundmass composed of the same phases plus Fe–Ti oxides (Fig. 2, Table 2). The lavas and scoriae of the intra-caldera cone contain small, partially disaggregated xenoliths of salic rocks. Xenoliths have granular texture and consist essentially of alkali feldspar granules that are strongly resorbed but are still recognizable as white coloured patches in hand specimen. This testifies to entrapment of silicic intrusive rocks.

The eccentric cone along the Gedemsa flank consists of strombolian scoriae and a lava flow, which show similar texture and composition to the intra-caldera rocks, except for the absence of xenocrystic alkali feldspars.

Trachytes and rhyolites

Silicic rocks mostly are peralkaline rhyolites, but the juvenile fractions of the ignimbrite (glassy fiamme and

Table 3: Major and trace element composition of Gedemsa rocks

	Wonji Basalts					Enclaves			
Sample:	GDCS1	GD65	GD3	GD80C	GD64	GD66	GD58	GD57	GD83B
SiO_2	47·50	48·19	49·95	50·20	51·65	51·21	51·89	52·38	52·40
TiO_2	1·89	2·01	1·86	1·83	2·15	1·87	1·61	1·69	1·82
Al_2O_3	14·40	16·90	16·30	16·54	16·98	18·15	18·95	18·00	17·36
Fe_2O_3	6·64	3·14	4·68	5·02	7·43	6·27	6·20	5·54	—
FeO	4·01	7·08	5·34	4·25	2·84	3·13	2·65	3·48	9·80
MnO	0·18	0·20	0·20	0·19	0·24	0·20	0·18	0·20	0·21
MgO	7·93	8·47	7·74	8·14	5·01	4·64	4·34	4·57	4·58
CaO	10·20	9·19	8·94	8·64	7·51	8·83	8·68	8·26	7·68
Na_2O	3·36	2·75	2·83	3·03	3·50	3·20	3·24	3·42	3·60
K_2O	1·15	0·89	1·21	1·20	1·07	1·36	1·18	1·49	1·48
P_2O_5	0·36	0·39	0·37	0·45	0·62	0·32	0·22	0·25	0·27
LOI	2·38	0·79	0·59	0·51	1·01	0·81	0·87	0·72	0·81
Mg no.	58·62	60·40	59·11	62·35	48·40	48·54	48·47	49·05	48·09
A.I.	0·47	0·32	0·37	0·38	0·41	0·37	0·35	0·40	0·43
V	241	284	256	212	203	212	92	217	207
Sc	—	26	28·8	25	27	21	14	20	22
Cr	360	227	332	354	34	95	27	81	79
Co	58	55	52	49	33	33	21	31	31
Ni	183	127	143	125	24	26	18	25	22
Rb	29	20	25	23	17	24	70	25	28
Sr	516	465	412	444	533	573	359	518	531
Ba	322	328	332	337	1096	524	848	743	565
Cs	—	0·2	0·1	—	0·1	0·6	0·1	0·5	0·38
Pb	12	2	8	4	14	5	18	7	11
Th	1	—	8	—	9	2	15	4	6
La	21	19	23	23	29	23	52	34	42
Ce	42	41	50	50	66	46	92	51	85
Nd	—	22	26	27	35	26	48	32	44
Sm	—	4·3	5·46	5·42	6·88	5·5	8·95	6·17	8·82
Eu	—	1·41	1·77	1·65	3·3	1·7	2·3	2·05	2·48
Tb	—	0·7	0·66	0·65	1	1	1·3	1	1·19
Yb	—	1·68	1·98	1·82	2·37	2·9	4·55	3·27	3·77
Lu	—	0·25	0·25	0·28	0·33	0·42	0·68	0·49	0·54
Y	27	22	26	24	34	31	65	59	54
Zr	193	147	159	164	179	156	397	175	237
Hf	—	2·8	4·18	3·7	3·4	3	7·3	3·4	5·1
Ta	—	1·3	1·57	1·6	1·4	1·4	2·8	1·3	2·1
Nb	33	26	27	28	32	28	65	31	43
Eu/Eu*	—	1	1·2	1·1	1·8	1	1	1·1	1·1

pumices) range from trachyte to rhyolite in the TAS diagram.

Pre-caldera rocks include lavas and pumices. Lavas have a weakly porphyritic texture (P.I. <5) with phenocrysts of anorthoclase, a few microphenocrysts of fayalite, and sporadic alkali pyroxene, amphibole and aenigmatite. The groundmass consists of texturally and compositionally homogeneous glass, in some cases with fluidal texture; there is no evidence of mingling with compositionally different magmas. Pumices are

Table 3: continued

	Enclaves						Pre-caldera rocks	
Sample:	GD82	GD13	GD55	GD10	GD56	GD15	GD4	GD17
SiO_2	52·66	54·41	55·92	57·85	59·64	60·30	67·18	67·55
TiO_2	1·81	1·34	1·41	1·99	1·22	1·17	0·52	0·37
Al_2O_3	16·57	19·53	17·26	13·87	15·47	15·30	13·36	11·15
Fe_2O_3	—	4·62	5·75	6·27	5·76	7·33	2·66	4·40
FeO	9·49	2·39	2·48	3·39	2·19	1·08	3·55	2·07
MnO	0·23	0·18	0·20	0·28	0·25	0·33	0·33	0·23
MgO	4·04	3·31	3·76	2·84	2·11	1·38	0·03	0·10
CaO	7·72	8·21	6·54	4·72	4·97	3·78	0·88	0·55
Na_2O	3·77	3·40	3·90	4·94	4·46	5·26	5·91	2·54
K_2O	1·72	1·40	1·95	2·21	2·62	2·93	4·76	4·38
P_2O_5	0·42	0·29	0·20	0·78	0·23	0·25	0·05	0·01
LOI	1·57	0·92	0·63	0·86	1·07	0·89	0·78	6·64
Mg no.	45·76	47·41	46·70	35·92	33·79	24·27	0·89	2·87
A.I.	0·49	0·36	0·49	0·76	0·66	0·77	1·11	0·80
V	133	128	152	113	204	61	9	9
Sc	—	17·4	15	24·2	19	29·9	—	1·8
Cr	41	42	65	7	84	19	5	5
Co	22	23	27	13	28	8	15	1
Ni	20	17	33	20	19	6	4	15
Rb	52	31	29	64	23	54	65	143
Sr	570	555	430	386	560	216	7	27
Ba	909	486	794	2790	503	1933	378	154
Cs	—	0·35	0·3	2·42	0·4	0·39	—	1·57
Pb	13	10	8	17	8	30	17	32
Th	5	5	3	17	5	11	14	27
La	49	31	93	101	35	41	46	98
Ce	101	69	65	203	50	91	88	214
Nd	—	30	87	85	37	43	—	85
Sm	—	6·86	15·6	18·7	7·02	9·13	—	17·1
Eu	—	2·24	3·67	6·23	2·05	3·32	—	2·52
Tb	—	0·95	2·7	2·97	1	1·21	—	2·52
Yb	—	2·9	6·75	8·73	3·43	4·02	—	10·4
Lu	—	0·4	0·98	1·2	0·49	0·45	—	1·45
Y	67	35	122	161	44	50	50	110
Zr	191	221	220	358	193	311	348	841
Hf	—	5·79	4·2	8·96	3·8	7·87	—	21·1
Ta	—	2·05	1·7	3·44	1·7	2·78	—	7·95
Nb	36	33	44	67	34	51	67	146
Eu/Eu*	—	1·2	1·1	1·7	1·1	1·5	—	0·7

nearly aphyric and consist of a homogeneous vesicular glass, sporadic microphenocrysts of anorthoclase, and rare alkali pyroxene, alkali amphibole and aenigmatite.

The ignimbrite is heterogeneous at the outcrop scale, in hand specimen and in thin section. The sampled deposit of the northeastern caldera rim is formed of a basal massive breccia, which grades into a stratified

	Pre-caldera rocks							
Sample:	GD21	GD35	GD22	GD23	GD24	GD19	GD5	GD20
SiO_2	68·00	68·30	69·70	70·21	71·27	71·59	72·49	72·87
TiO_2	0·40	0·36	0·36	0·34	0·32	0·37	0·37	0·34
Al_2O_3	9·72	10·30	9·88	9·68	9·05	10·46	8·95	9·27
Fe_2O_3	3·71	3·61	3·94	4·65	3·49	6·69	3·11	3·39
FeO	1·96	2·08	1·71	1·38	1·98	0·40	3·87	3·12
MnO	0·19	0·19	0·21	0·22	0·21	0·27	0·30	0·24
MgO	0·15	0·12	0·11	0·13	0·13	0·13	0·01	0·01
CaO	0·93	0·35	0·47	0·37	1·03	0·47	0·26	0·24
Na_2O	1·54	3·37	2·16	2·24	1·73	4·07	5·80	5·61
K_2O	4·89	4·90	4·16	3·99	4·98	4·32	4·15	4·22
P_2O_5	0·03	0·03	0·03	0·01	0·01	0·02	0·01	0·01
LOI	8·48	6·39	7·27	6·79	5·81	1·21	0·70	0·68
Mg no.	4·80	3·86	3·60	4·00	4·33	3·48	0·27	0·29
A.I.	0·80	1·05	0·81	0·83	0·91	1·09	1·56	1·49
V	9	8	9	9	9	9	9	9
Sc	0·9	1·4	0·8	0·8	0·7	0·7	0·6	0·7
Cr	3	2	1	0	4	3	4	1
Co	1	10	3	2	1	11	3	1
Ni	18	10	14	19	14	23	15	16
Rb	149	137	132	147	132	116	136	147
Sr	20	10	34	20	36	55	3	3
Ba	121	146	131	121	105	161	123	123
Cs	1·85	1·63	1·9	1·92	1·7	1·8	1·88	1·93
Pb	29	62	43	28	24	32	23	26
Th	25	—	39	31	28	32	27	28
La	107	102	107	110	97	149	106	110
Ce	231	224	245	242	221	264	226	246
Nd	96	88	99	100	91	114	97	95
Sm	19·6	19·1	21·9	22·3	20	27	20	20·6
Eu	2·77	2·61	2·91	2·95	2·64	3·9	3·33	3
Tb	2·93	2·61	3·09	3·1	2·77	4·04	2·94	2·2
Yb	11·4	10·7	11·4	11·6	10·8	14·7	11·3	11·9
Lu	1·44	1·16	1·56	1·47	1·1	1·49	1·1	1·69
Y	112	87	108	113	104	163	132	116
Zr	869	699	784	869	765	1016	782	846
Hf	21·3	20·7	20·3	21·6	18·7	21·2	19·7	21·1
Ta	8·61	9·24	9·44	9·92	8·82	8·73	8·3	8·53
Nb	155	94	141	159	141	191	153	153
Eu/Eu*	0·7	0·7	0·7	0·7	0·7	0·8	0·9	0·9

top. The juvenile component consists of moderately to strongly porphyritic glass fiamme (phenocryst contents 20–50%), with phenocrysts of alkali feldspar, fayalite, and sporadic alkali pyroxene, aenigmatite, biotite and Fe–Ti oxides, set in a glassy matrix. In most samples alkali feldspars are strongly corroded, indicating a xenocrystic origin.

The post-caldera silicic rocks have variable textures. Some are porphyritic with phenocrysts of sanidine–anorthoclase and minor plagioclase, biotite, alkali pyroxene and aenigmatite set in a hypocrystalline to glassy groundmass; other rocks are almost totally vitreous with accessory amounts of sanidine–anorthoclase microphenocrysts. Pumice samples are

Table 3: continued

	Post-caldera rocks							
Sample:	GD2	GD8	GD18	GD7	GD6	GD9	GD16	GD12
SiO_2	66·97	69·10	69·19	69·33	69·83	70·68	71·69	72·18
TiO_2	0·59	0·43	0·18	0·51	0·18	0·41	0·16	0·19
Al_2O_3	11·97	10·40	7·54	12·43	7·55	10·98	7·95	8·27
Fe_2O_3	6·62	5·94	5·50	3·99	8·12	5·30	4·85	4·56
FeO	0·15	0·59	2·36	1·90	0·05	1·57	3·35	3·29
MnO	0·22	0·28	0·30	0·21	0·31	0·30	0·33	0·31
MgO	0·83	0·06	0·07	0·78	0·02	0·08	0·08	0·02
CaO	1·93	1·29	0·71	1·39	0·27	0·68	0·30	0·23
Na_2O	5·13	5·41	3·58	5·06	4·44	4·98	6·03	6·42
K_2O	3·99	4·50	5·34	3·91	5·15	4·34	4·01	4·04
P_2O_5	0·10	0·03	0·01	0·06	0·01	0·01	0·01	0·01
LOI	1·50	1·97	5·21	0·44	4·08	0·68	1·24	0·51
Mg no.	19·51	1·77	1·68	20·21	0·48	2·20	1·82	0·48
A.I.	1·05	1·32	1·55	1·01	1·70	1·17	1·79	1·80
V	28	9	9	24	9	9	9	9
Sc	5·9	2·6	0·2	5·9	0·7	2·7	0·2	0·7
Cr	14	1	2	12	1	4	3	3
Co	6	1	2	6	2	7	2	5
Ni	17	10	24	12	37	9	27	35
Rb	122	119	177	116	242	129	171	225
Sr	89	69	79	102	9	18	13	6
Ba	337	403	225	327	280	410	236	265
Cs	0·5	0·43	2·01	0·78	3·13	0·69	3·11	2·91
Pb	30	23	36	18	44	25	31	45
Th	25	21	30	12	42	20	25	44
La	91	80	146	90	204	86	159	192
Ce	196	174	323	181	446	169	348	411
Nd	81	73	132	77	190	75	156	160
Sm	17·2	15·1	29·3	16·7	38·1	15·3	31	35
Eu	3·35	3·4	5·48	3·21	5·94	3·33	6·04	5·6
Tb	2·61	2·32	4·42	2·28	5·74	2·21	4·95	5·46
Yb	9·78	9·16	16·1	8·26	21·1	7·73	17·8	20·3
Lu	1·2	1·1	1·76	1·05	2·5	0·95	2·2	2·2
Y	101	101	175	90	243	86	204	217
Zr	734	674	1104	650	1560	665	1251	1565
Hf	17·8	15·9	27·9	17·7	38·5	16·9	29·7	35
Ta	6·38	6·32	10·9	6·49	14·3	6·27	11·8	13·5
Nb	123	108	196	107	260	113	223	263
Eu/Eu*	1	1·1	1·1	1	1	1	1·2	1

vesicular and contain small amounts of sanidine–anorthoclase, alkali pyroxene, aenigmatite and biotite. As discussed below, mingled textures with mafic magmas are commonly observed in the post-caldera rhyolites.

Porphyritic mafic–intermediate enclaves

Enclaves of mafic to intermediate composition have been found in some post-caldera products, and are particularly abundant along the eastern rim of the Kore crater. They occur either as dark centimetre- to

	Ignimbrites						
Sample:	GD30	GD37	GD74A	GD32	GD29	GDCS2	GD34
SiO_2	62·01	64·70	65·69	65·80	67·19	70·50	71·64
TiO_2	0·79	0·80	0·84	0·63	0·64	0·28	0·18
Al_2O_3	13·56	12·73	12·00	12·46	11·40	9·25	8·13
Fe_2O_3	7·69	6·13	—	5·18	7·48	6·40	5·29
FeO	0·99	2·53	8·74	2·25	0·64	0·75	3·14
MnO	0·52	0·45	0·40	0·40	0·37	0·27	0·32
MgO	0·18	0·40	0·46	0·27	0·20	0·06	0·03
CaO	1·95	1·72	1·46	1·80	1·27	0·36	0·27
Na_2O	5·96	5·46	5·97	5·44	5·62	3·40	6·12
K_2O	4·30	3·89	3·73	4·39	4·28	4·38	3·99
P_2O_5	0·10	0·10	0·12	0·07	0·07	0·03	0·01
LOI	1·96	1·10	0·58	1·31	0·84	4·32	0·88
Mg no.	3·90	8·14	9·44	6·51	4·61	1·61	0·67
A.I.	1·07	1·03	1·15	1·10	1·22	1·12	1·77
V	9	10	13	9	9	8	9
Sc	18·8	21·1	15	7·3	8·8	0·4	2·1
Cr	11	2	4	6	6	2	6
Co	12	8	1	6	1	3	3
Ni	7	4	3	5	8	37	27
Rb	53	59	75	74	111	230	170
Sr	65	37	71	63	42	12	11
Ba	2903	2847	2303	899	1105	380	233
Cs	0·42	—	—	0·39	0·57	2·11	2·45
Pb	14	12	16	13	36	42	31
Th	12	11	11	16	26	33	31
La	36	48	58	54	77	111	163
Ce	80	107	118	114	163	263	376
Nd	48	47	63	63	83	115	157
Sm	11·7	10·9	13	12·4	17·3	23·8	36
Eu	4·5	3·84	3·86	3·2	4·1	5·2	5·65
Tb	1·57	1·46	1·67	1·56	2·38	4·21	5·13
Yb	5·15	4·93	5·81	5·77	8·52	15·24	18·4
Lu	0·59	0·65	0·88	0·72	0·74	1·55	1·53
Y	66	60	58	52	92	210	171
Zr	283	358	485	408	657	1488	1185
Hf	6·5	9·1	10·9	10	13·9	25·7	31·3
Ta	3·04	3·9	4·3	4·63	6·78	12·5	13·8
Nb	58	65	78	76	118	218	212
Eu/Eu*	1·7	1·5	1·4	1·2	1·2	1·1	1

Mg no. $= 100 \times Mg/(Mg + Fe^{2+})$ atomic ratio, assuming $Fe^{2+}/Fe_{total} = 0{\cdot}85$. Eu* is Eu concentration extrapolated from smooth REE patterns. A.I., Agpaitic Index [molecular $(Na_2O + K_2O)/Al_2O_3$]. —, not determined.

decimetre-sized blobs with irregular, crenulated margins (Fig. 3a) or as millimetre-sized blebs dispersed in the rhyolitic rock. Isolated feldspar phenocrysts with rims of mafic matrix are commonly found dispersed in the rhyolite (Fig. 3b). In the northern flank of the Kore cone (Fig. 1), enclaves form a deposit a few metres thick of vesicular globules that are surrounded by, and partially intermingled

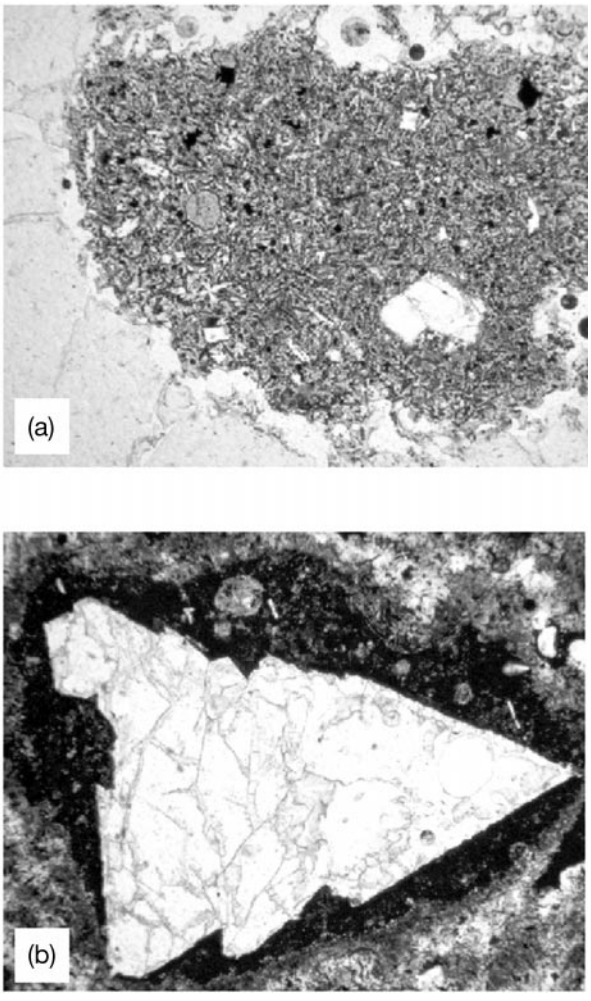

Fig. 3. Microstructures of mingled lavas from the Gedemsa post-caldera volcanics. (a) Contacts between mafic lava and silicic host (parallel polars, 10×). (b) Large phenocryst (about 1 cm) of plagioclase with a jacket of mafic material in a rhyolitic rock (parallel polars, 10×).

with an approximately equal amount of rhyolitic material.

The enclaves are moderately to strongly porphyritic (phenocryst contents 10–30%), with large euhedral phenocrysts of predominantly plagioclase, along with minor clinopyroxene and olivine. Mafic to intermediate enclaves are homogeneous in texture and do not show significant petrographic evidence of disequilibrium, such as reaction rims around phenocrysts or mineral corrosion. In the most mafic enclaves, olivine is typically Fo_{80}, plagioclase is bytownite–labradorite, and clinopyroxene ranges from diopside to augite. Enclaves with an intermediate composition have olivine with lower forsterite contents ($Fo_{70–50}$), andesine–bytownite plagioclase, and diopside–augite clinopyroxene. Some of the intermediate enclaves contain large xenocrysts of alkali feldspar, which show strongly corroded borders. Some enclaves consist of intermingled mafic and rhyolitic material and show extremely heterogeneous mineral compositions, with the occurrence of phenocrysts and partially resorbed xenocrysts of Mg-rich olivine, fayalite, diopside, Ca-plagioclase, anorthoclase and sanidine; these enclaves have not been considered further, because of the difficulty in separating mafic and silicic components for geochemical analysis.

The textural relationships described above clearly suggest that the porphyritic enclaves represent blobs of mafic to intermediate magma, which interacted with the rhyolitic melt. This testifies to the contemporaneous presence of mafic, intermediate and silicic magma within the volcanic system.

GEOCHEMISTRY

Analytical methods

About 70 samples have been analysed for major and trace elements. These include lava and pumice from the pre-caldera sequence, the juvenile fraction of syn-caldera ignimbrite, post-caldera lavas and pumices, enclaves from post-caldera rhyolites, and scoria and lava samples from late basalts along the Wonji fault. Samples were crushed in a steel jaw crusher and reduced to a fine powder in agate mortars. Mingled silicic rocks were checked carefully after reduction to chips, to avoid mafic material being accidentally ground with silicic. The same procedure was adopted for juvenile components of the ignimbrite. The samples of enclaves were extracted from the host rock in the field by hammering and drilling, trying to avoid the silicic host rock.

Major elements and Ba, Rb, Sr, Y, Zr and Nb were analysed by combined X-ray fluorescence and wet chemical techniques [Na_2O, FeO and loss on ignition (LOI)] at the Department of Earth Sciences, University of Perugia. Rare earth elements (REE), Th, U, Cs, Ta, Hf, Sc and Co were analysed by instrumental neutron activation analysis at the Department of Geology of the University of Western Ontario, Canada. Precision is better than 10% for all the elements. Sr and Nd isotopic ratios were determined at Centro di Studio per il Quaternario e l'Evoluzione Ambientale (CNR, Rome) at the Department of Earth Sciences, University of Rome 'La Sapienza', using a VG54E mass spectrometer. Precision (2σ) is better than ± 2 in the fifth decimal place for both Sr and Nd isotopes. Pb isotope ratios were determined at Carleton University, Ottawa, using a Finnigan-MAT multi-collector mass spectrometer. All Pb isotope ratios were adjusted to the absolute value of reference standard NBS 981 given by Todt *et al.* (1995). Further details on the analytical

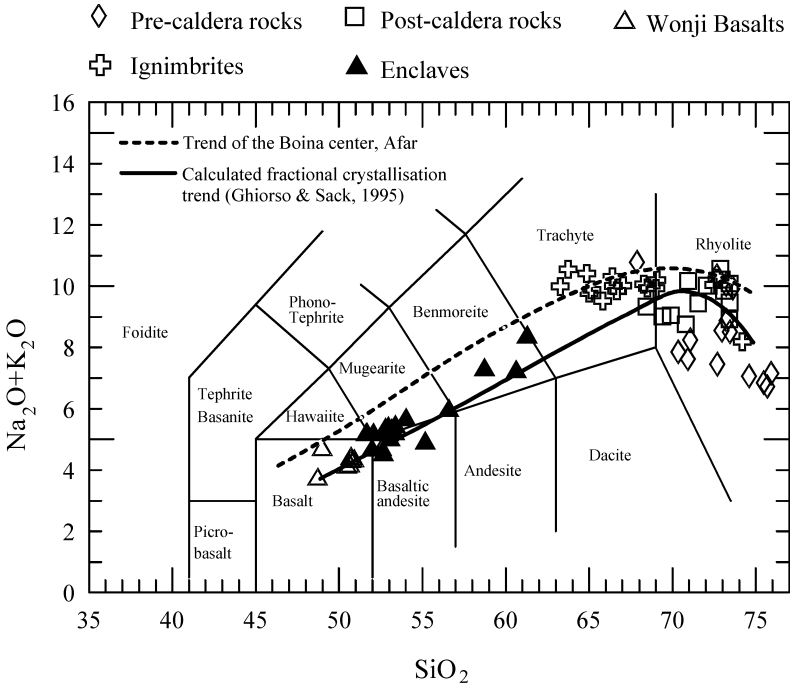

Fig. 4. TAS classification diagram for the Gedemsa volcanics. Data recalculated to 100% on a water-free basis. The dashed curve reproduces compositional variations of rocks from the Boina centre, Afar (Barberi *et al.*, 1975). The continuous curve represents a fractional crystallization model calculated according to Ghiorso & Sack (1995).

methods have been reported by Bell & Tilton (2001). Precision is 0·04%. Oxygen isotopic compositions on separated phases were determined at the Geochron Laboratories, Cambridge, MA, USA. Values were reported in δ‰ with respect to SMOW. The $^{18}O/^{16}O$ of the standard was 0·0039948. Precision is ±2 in the first decimal place.

Major element, trace element and isotopic data for the analysed samples are reported in Tables 3 and 4.

Results

Major elements

A total alkali vs silica (TAS) classification diagram (Fig. 4) shows that both the pre- and post-caldera products consist of rhyolites, with the syn-caldera ignimbrite mostly displaying trachytic compositions. The Wonji lavas and scoriae have a typical transitional basalt composition, whereas the enclaves from the post-caldera rhyolites range from basalt to benmoreite. If the enclaves are excluded, the bulk of the rocks typically show a bimodal distribution of compositions with a wide Daly Gap, as observed at a regional scale along the Ethiopian rift. Silicic rocks are peralkaline and can be mostly classified as pantellerites, with a few comendites and trachytic pantellerites (Macdonald, 1974).

Harker diagrams are shown in Fig. 5. There is a continuous decrease in MgO, FeO_t, CaO, TiO_2, Al_2O_3 and P_2O_5, and an increase in K_2O with increasing silica. Na_2O increases from basalt to trachyte, and then decreases sharply in the rhyolites. MnO clusters around 0·2–0·3 wt %, but some ignimbrite samples display much higher values, up to about 0·6 wt % (Table 3). Overall, the Gedemsa rocks display major element variation trends similar to those from the Boina centre, Afar (Barberi *et al.*, 1975).

Trace elements

Trace element diagrams (Fig. 6) display negative correlation for Co and Cr vs SiO_2. Except for a few samples, enclaves plot along curved trends between the basalts and silicic rocks. Negative trends are also observed for Sr, V, Ni and Sc (not shown). Incompatible trace elements, such as Nb, Zr, REE, etc. increase with silica, although extremely high values such as those observed in the Naivasha rhyolites (Macdonald *et al.*, 1987) are not observed. Ba increases slightly from the basalts to intermediate enclaves, shows very high values in some trachytic ignimbrite samples and two enclaves, and decreases sharply in the rhyolites.

Incompatible element vs incompatible element diagrams show smooth linear positive trends that pass through the origin (Fig. 7), although the REE contents of some enclaves are notable exceptions (Fig. 7c). Post-caldera rhyolites range to more enriched compositions

Table 4: Sr, Nd, Pb and oxygen isotope data for selected volcanic rocks from Gedemsa

	Wonji Basalts			Enclaves			
Sample:	GDCS1	GD3	GD82	GD13	GD10	GD15	GD 83B
$^{87}Sr/^{86}Sr$	0·704080	0·704047	0·704184	0·704534	0·704437	0·704766	0·704200
$^{87}Sr/^{86}Sr_{initial}$	0·704079	0·704046	0·704083	0·704533	0·704435	0·704763	0·704199
$^{143}Nd/^{144}Nd$		0·512795			0·512786		
$^{206}Pb/^{204}Pb$		18·296					
$^{207}Pb/^{204}Pb$		15·576					
$^{208}Pb/^{204}Pb$		38·512					
$\delta^{18}O$		+5·8 (olivine)		+6·8 (alkali feldspar)	+7·9 (alkali feldspar)		

	Pre-caldera rocks				
Sample:	GD4	GD21	GD35	GD22	GD24
$^{87}Sr/^{86}Sr$	0·706115	0·706905	0·706945	0·707188	0·706938
$^{87}Sr/^{86}Sr_{initial}$	0·705993	0·706807	0·706765	0·707137	0·706900
$^{143}Nd/^{144}Nd$	0·512794			0·512739	
$^{206}Pb/^{204}Pb$	18·324				
$^{207}Pb/^{204}Pb$	15·581				
$^{208}Pb/^{204}Pb$	38·571				

	Post-caldera rocks			Ignimbrite			
Sample:	GD8	GD6	GD12	GD29	GDCS2	GD34	GD27
$^{87}Sr/^{86}Sr$	0·704062	0·706834	0·706604	0·705645	0·704794	0·706790	0·704399
$^{87}Sr/^{86}Sr_{initial}$	0·704043	0·706547	0·706203	0·705617	0·704590	0·706630	0·704387
$^{143}Nd/^{144}Nd$	0·512796		0·512795	0·512775		0·512779	
$^{206}Pb/^{204}Pb$	18·276		18·135				
$^{207}Pb/^{204}Pb$	15·549		15·554				
$^{208}Pb/^{204}Pb$	38·458		38·390				
$\delta^{18}O$	+6·2 (alkali feldspar)	+7·3 (alkali feldspar)					

During this study the La Jolla standard gave an average value of $^{143}Nd/^{144}Nd = 0{\cdot}51185 \pm 0{\cdot}00002$ and the NBS 987 standard gave an average value of $^{87}Sr/^{86}Sr = 0{\cdot}71024 \pm 0{\cdot}00002$. Initial Sr isotopic compositions have been calculated at 0·32 Ma for pre-caldera rocks and at 0·26 Ma for ignimbrite and post-caldera rocks. Oxygen isotopic data are on separated minerals (indicated in parentheses).

than pre-caldera rhyolites. The ignimbrite has a very variable incompatible element composition, ranging from values slightly higher than those of basalts to high concentrations like those of the most fractionated rhyolites. Therefore, there is a very small compositional gap between basalts and trachytes in the distribution of incompatible trace elements. Ratios of incompatible elements such as Rb/Nb, Th/Ta, La/Lu and La/Sm (not shown) are somewhat scattered, but do not show significant variations from basalt to trachytes and rhyolites.

REE patterns are all fractionated but do not display significant differences in the degree of fractionation (Fig. 8). Negative Eu anomalies are observed in the peralkaline rhyolites and some of the trachytes. Other trachytes have smooth REE patterns and do not show

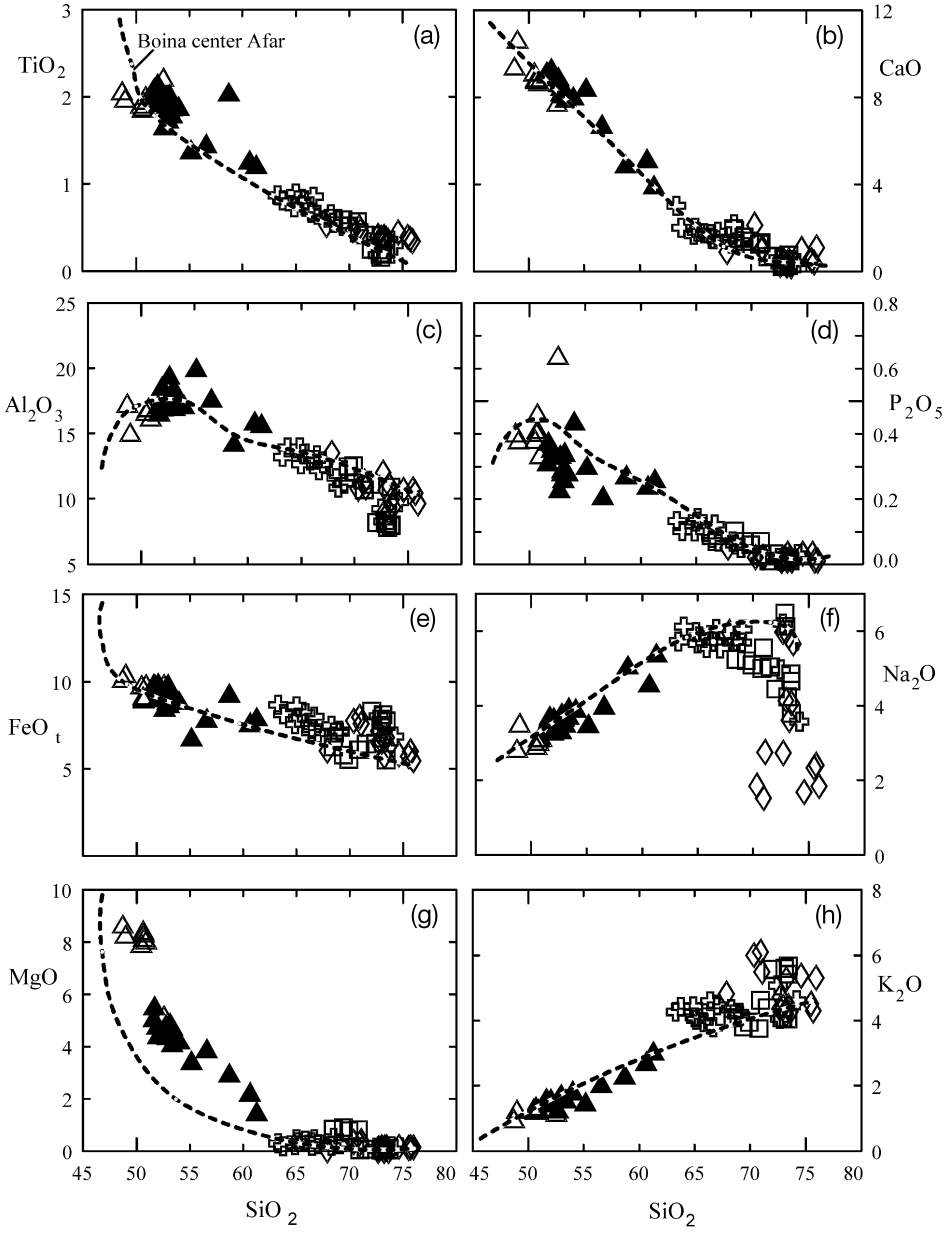

Fig. 5. Major element Harker diagrams. The dashed curve represents the compositional variation of the Boina centre, Afar (Barberi *et al.*, 1975). Data recalculated on a water-free basis. Symbols as in Fig. 4.

Eu anomalies; it should be noted that these later rocks are all rich in Ba. Some of the enclaves in the post-caldera rhyolites exhibit an anomalous behaviour for some REE. They display comparable Ce and Eu concentrations to the basalts, but have higher concentrations of other REE; as a consequence, negative Ce and Eu anomalies appear on chondrite-normalized REE plots (Fig. 8b), and REE abundances, except Ce and Eu, fall outside smooth patterns on inter-element variation diagrams (Figs 6 and 7).

Sr, Nd, Pb, O isotopes

Measured Sr isotope ratios range from 0·70041 to 0·70719. There is an overall increase of $^{87}Sr/^{86}Sr_{initial}$ with silica (Fig. 6h), although some silicic rocks have Sr isotope ratios similar to those of basalts. Feldspars separated from the pre-caldera obsidian GD4 have measured $^{87}Sr/^{86}Sr = 0{\cdot}70519$, significantly lower than the host rock ($^{87}Sr/^{86}Sr = 0{\cdot}70612$; $^{87}Sr/^{86}Sr_{initial} = 0{\cdot}70599$) (Table 4). Nd isotopic compositions are much less variable and cluster around 0·51274–0·51279.

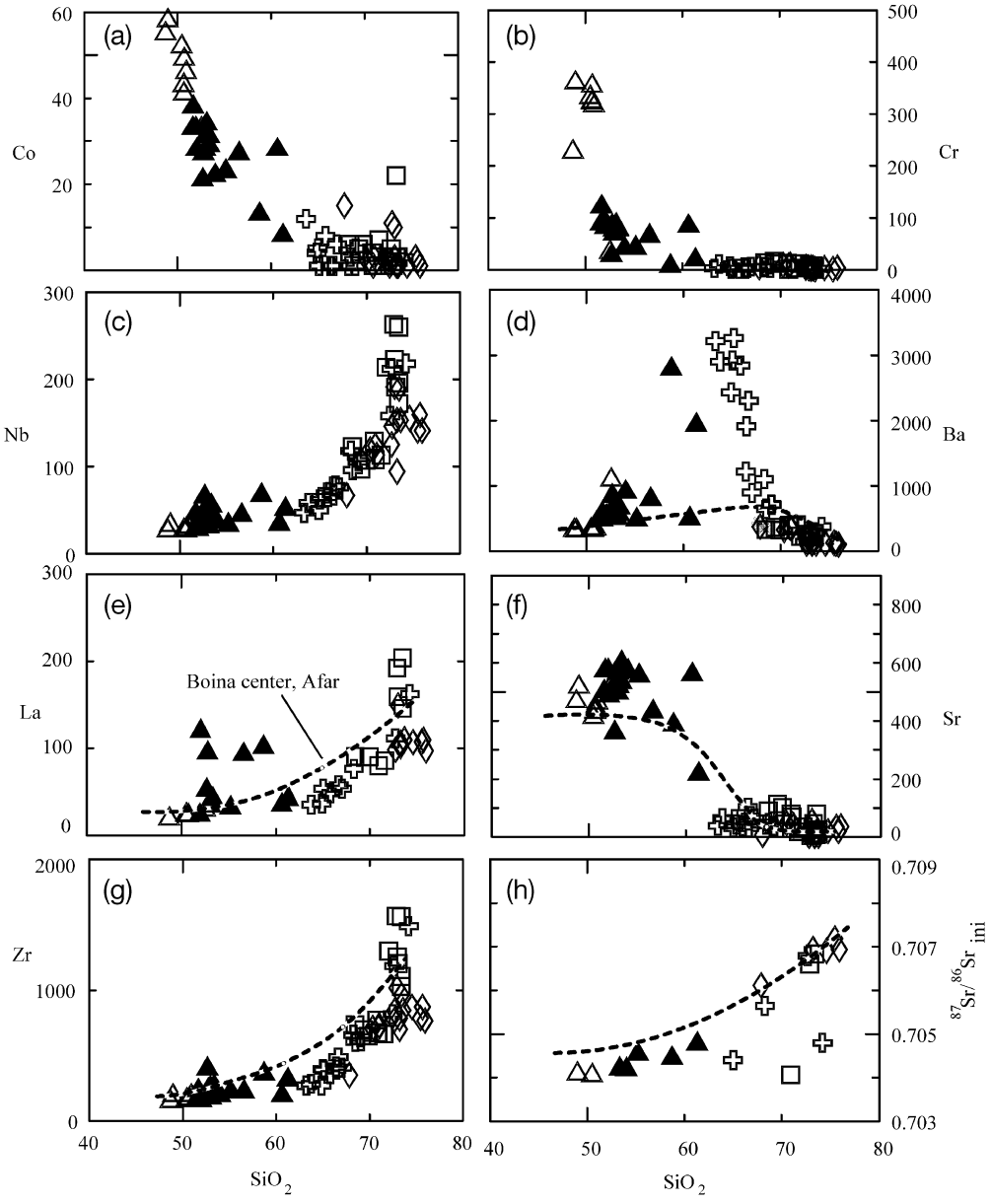

Fig. 6. Variation diagrams of trace elements and $^{87}Sr/^{86}Sr$ vs SiO_2. The dashed curve represents the compositional variation of the Boina centre, Afar (Barberi *et al.*, 1975). Symbols as in Fig. 4.

The mafic samples plot in the field of Afar and Main Ethiopian Rift volcanics on the Sr–Nd isotope diagram (Hart *et al.*, 1989; Deniel *et al.*, 1994; Trua *et al.*, 1998), whereas silicic rocks plot outside this field, because of more radiogenic Sr compositions (Fig. 9a). Pb isotope ratios (Fig. 9b) fall in the field of the Ethiopian rift volcanics (Hart *et al.*, 1989; Trua *et al.*, 1998).

Oxygen isotope ratios of minerals separated from rocks with variable compositions range from +5·8 (olivine from GD3 basalt) to +7·9 (alkali feldspar from GD22 rhyolite). When magmatic values are calculated from mineral compositions, this range becomes considerably smaller, with basaltic magma having $\delta^{18}O‰ = +6{\cdot}2$ and GD22 rhyolite having $\delta^{18}O‰ = +7{\cdot}4$ (assuming a basalt–olivine fractionation of 0·4‰, and a rhyolite–alkali feldspar fractionation of −0·5‰; Appora *et al.*, 2003).

Comments on some anomalous element concentrations

Some of the investigated rocks show unusual geochemical signatures, which must be understood before using

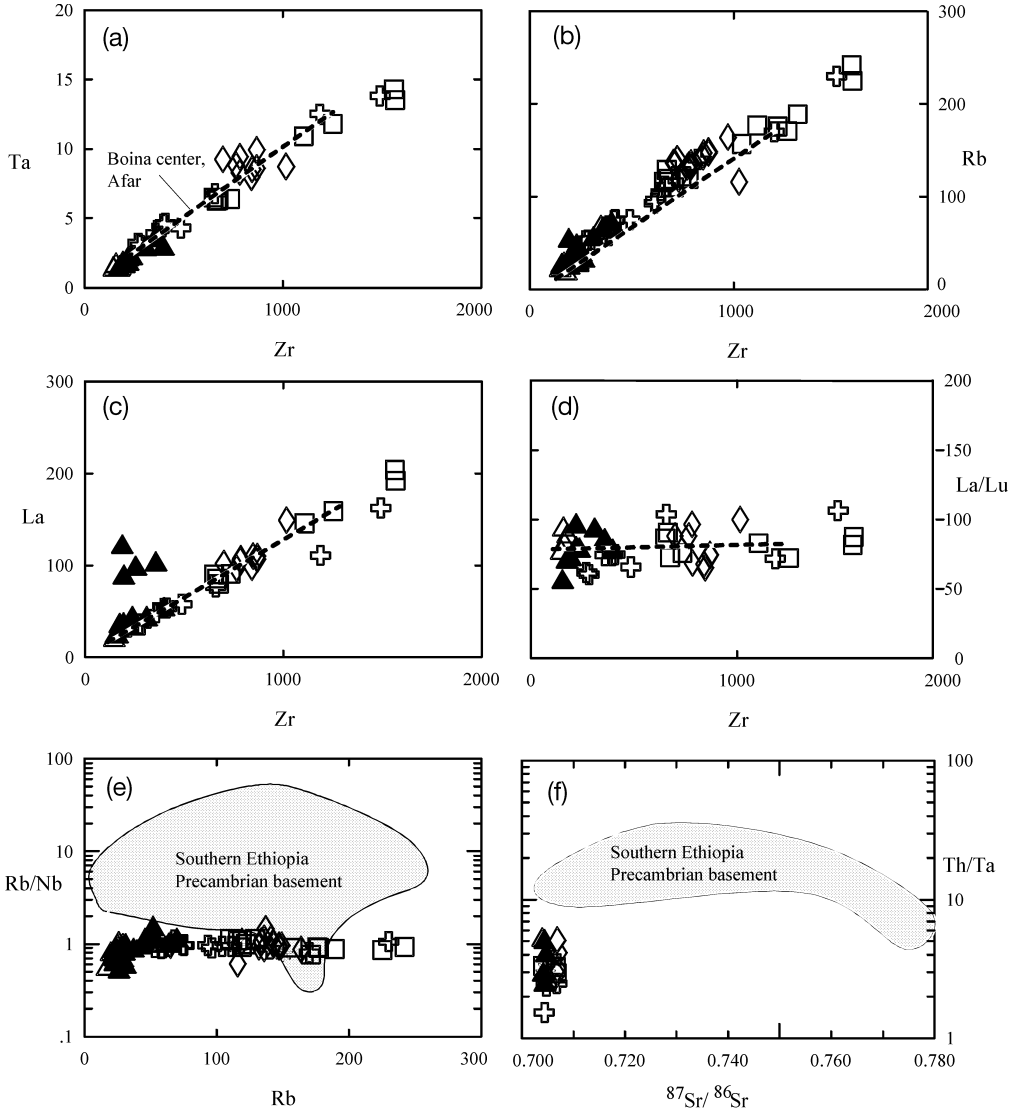

Fig. 7. Variation diagrams for incompatible element abundance and ratios, and for $^{87}Sr/^{86}Sr$. Data for Precambrian basement are from Peccerillo *et al.* (1998). Symbols as in Fig. 4.

rock compositions to model petrogenetic processes. These include the negative Ce anomalies of some enclaves, the high Ba contents of some trachytes and the low Na_2O of some rhyolites.

One group of enclaves has higher REE contents (except Ce and Eu) than rocks with the same degree of evolution (comparable SiO_2 and MgO wt %). These have negative Ce and Eu anomalies in the REE patterns (Fig. 8). Negative Ce anomalies have been found in basaltic rocks from several volcanic provinces, including the Ethiopian rift (Trua *et al.*, 1998), and have generally been attributed to either deuteric processes or assimilation of rocks with negative Ce anomalies (e.g. ferruginous sediments; Cotten *et al.*, 1995; Bohrson & Reid, 1997). However, Ce-depleted sedimentary rocks are unlikely to be present in the rift, which, on the basis of field evidence, seems to consist entirely of volcanic rocks sitting on metamorphic basement. Moreover, the analysed enclaves do not show evidence for significant secondary alteration and some of them have low LOI values. It must be noted that Ce and Eu are the only elements of the REE group that display concentrations that are comparable with those of other rocks with the same degree of evolution and plot on smooth linear trends on inter-element variation diagrams. In other words, these enclaves do not show negative anomalies of Ce and Eu, but rather high values of all the other REE. We suggest that an

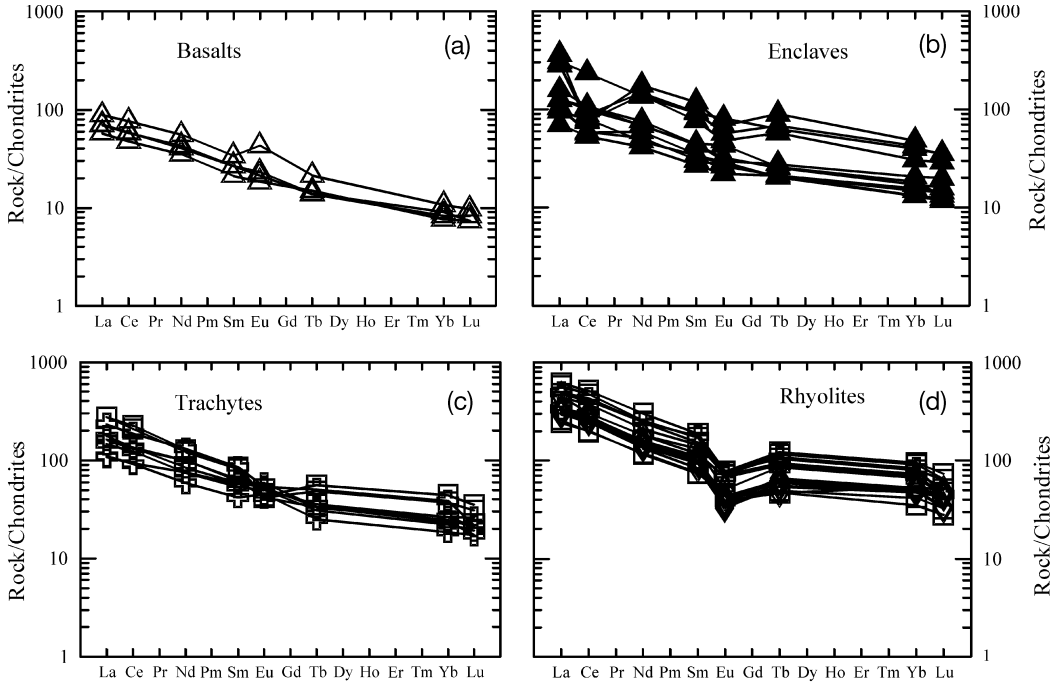

Fig. 8. REE patterns of the Gedemsa rocks. Normalizing values after Nakamura (1974).

alternative explanation for the anomalous REE concentrations may be related to differential diffusion of these elements from host rhyolite to the mafic magma. Studies on diffusivity in silicate melts have provided evidence for complex behaviour, as a function of various factors such as element charge and ionic radius, silicate melt structure, temperature and pressure (e.g. Nakamura & Kushiro, 1998; Mungall, 2002). Nakamura & Kushiro (1998) suggested that negative spikes of Eu could be generated by differential REE diffusion at the contact between mafic and silicic magmas. The same process can affect Ce, which can be at +4 valence in oxidizing conditions. It is beyond the scope of this paper to discuss in detail these problems. However, we wish to emphasize that some of the analysed enclaves do not preserve compositions of original liquids for some elements, whose abundance may have been strongly and selectively modified by diffusion. Therefore the composition of these samples will not be used in petrological modelling.

Some syn-caldera ignimbrite samples and two intermediate enclaves have exceedingly high concentrations of Ba (Fig. 6d). These are difficult to explain by common magmatic processes, such as fractional crystallization, magma mixing or partial melting. Figure 10 shows that there are positive correlations between Ba, MnO, FeO_{total} and Eu/Eu*. Mineral chemistry data (Table 2) have shown that fayalite from silicic rocks has high MnO contents (up 6 wt %). Moreover, some alkali feldspars have high BaO contents (up to 2·5–3·0 wt %). Therefore, we believe that accumulation of these phases may have produced an increase in Ba and MnO in the Ba–Mn-rich magmas. This is supported by the strongly porphyritic texture of the Ba-rich rocks and by large crystals of alkali feldspar and fayalite that are often corroded, indicating a xenocrystic nature. A positive correlation between Ba and Eu/Eu* (see Fig. 10a and c), supports accumulation of alkali feldspar. On the other hand, the positive correlation between MnO and FeO_{total} (Fig. 10b) supports fayalite accumulation. Simple mass balance calculations show that some 10% accumulation of BaO-rich alkali feldspar (about 7%) plus MnO-rich fayalite (about 3%) can explain the anomalous Ba and MnO concentration of the trachytes. This is a minimum estimate, and the amounts of cumulate phases are much higher if less Ba–Mn-rich compositions for olivine and alkali feldspar are assumed. The strongly porphyritic texture of these rocks (up to 50% phenocrysts or xenocrysts) also has other effects on the whole-rock chemistry. First, feldspar accumulation is responsible for both high Ba and the lack of negative Eu anomalies in the REE patterns. Moreover, elements that are not hosted in the accumulated phases become strongly diluted, although their ratios may not change significantly. Element dilution is supported by a negative correlation between Eu/Eu* and trace element abundances (e.g. Zr, La, etc.; not shown), and can

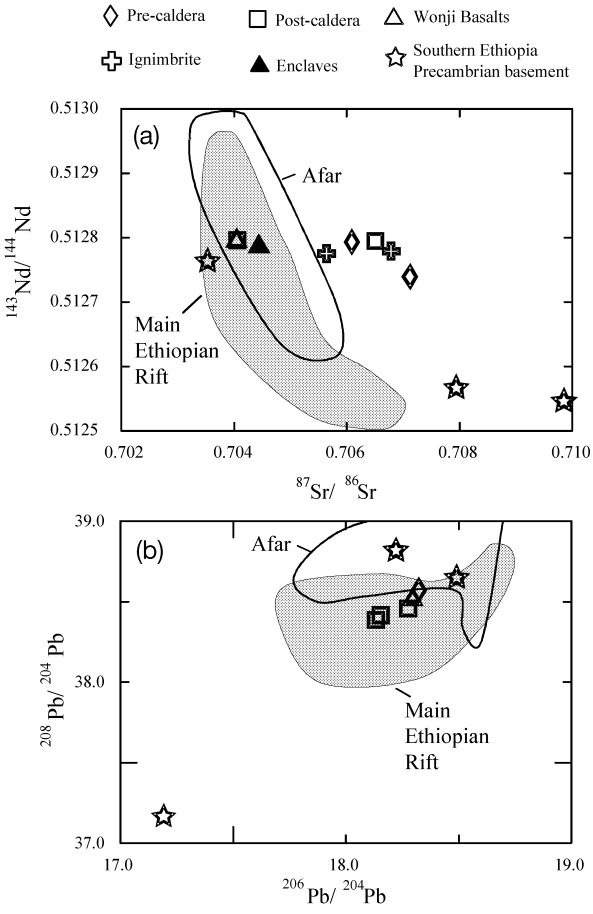

Fig. 9. Sr, Nd, and Pb isotope variation diagrams. Data for Afar and Ethiopian rift are from Hart *et al.* (1989), Deniel *et al.* (1994) and Trua *et al.* (1998). Data for Precambrian basement rocks are from Peccerillo *et al.* (1998) and authors' unpublished data.

explain why the trace element abundances of Ba-rich trachytes are close to those of basalts, reducing the chemical gap between mafic and silicic rocks. Thus, petrographic and geochemical evidence strongly suggests that the Ba-rich rocks do not represent liquids; therefore, their composition will not be considered in trace element modelling discussed below.

Finally, a large variation in Na_2O is observed in the rhyolites. Major element modelling suggests that this range can only partially be explained by Na-feldspar fractionation; however, exceedingly low values are found in some samples (generally pumices). There is a negative correlation between Na_2O and LOI for some silicic rocks (Fig. 10d), which clearly suggests that the loss of sodium was accompanied by an increase in volatiles, mostly water. This clearly points to a deuteric process, probably leaching by surface waters of the glass (see Yirgu *et al.*, 1999). However, lack of correlation between LOI and any other major and trace element (not shown) indicates that deuteric transformations did not affect the concentrations of other elements.

DISCUSSION

The main problems of the Gedemsa volcano include explaining the origin of peralkaline silicic rocks, their relationship with basaltic magmas, and the reasons for the paucity of mafic and intermediate compositions in the volcanic sequence. It should be noted that the problem of the genesis of silicic melts, their relationship with associated basalts, and the nature of the Daly Gap holds also for several subalkaline provinces such as Iceland, Paranà, Deccan, Yemen, etc. (Bellieni *et al.*, 1985; Thy *et al.*, 1990; Chazot & Bertrand, 1995; Garland *et al.*, 1995; Streck & Grunder, 1997).

Two classes of hypotheses have been proposed to explain silicic peralkaline volcanism. One suggests continuous fractional crystallization starting from transitional basaltic parents, possibly with a role for crustal contamination (e.g. Barberi *et al.*, 1975; Gasparon *et al.*, 1993; Geist *et al.*, 1995; Mungall & Martin, 1995; Civetta *et al.*, 1998). The other suggests that peralkaline silicic rocks and the associated basalts represent two genetically independent melts, with the basalts coming from the mantle and the silicic liquids being generated in the crust, by melting of either old crust or young underplated basalts (e.g. Davies & Macdonald, 1987; Lightfoot *et al.*, 1987; Macdonald *et al.*, 1987; Mahood *et al.*, 1990; Black *et al.*, 1997; Bohrson & Reid, 1997; Trua *et al.*, 1998).

The fractional crystallization hypothesis is able to explain several geochemical and isotopic features of mafic–silicic rocks, notably in the Afar and at Pantelleria (Barberi *et al.*, 1975; Civetta *et al.*, 1998; but note Lowenstern & Mahood, 1991), but introduces the problem that large volumes of basaltic magma are needed to produce the silicic rocks and fails to explain the lack of intermediate rocks (Daly Gap). Both of these objections are particularly relevant in the Ethiopian rift, where intermediate rocks are rare to absent, silicic peralkaline volcanic rocks are extremely abundant and basalts occur in small amounts (e.g. Mohr, 1971; Di Paola, 1972). In contrast, the crustal melting hypotheses nicely explain the Daly Gap and the dominance of silicic rocks (e.g. Macdonald *et al.*, 1987; Bohrson & Reid, 1997; Trua *et al.*, 1998).

The data obtained in this study will be discussed with the aim of providing constraints on the genesis of the Gedemsa peralkaline rocks and to explore the implications for Ethiopian rift volcanism.

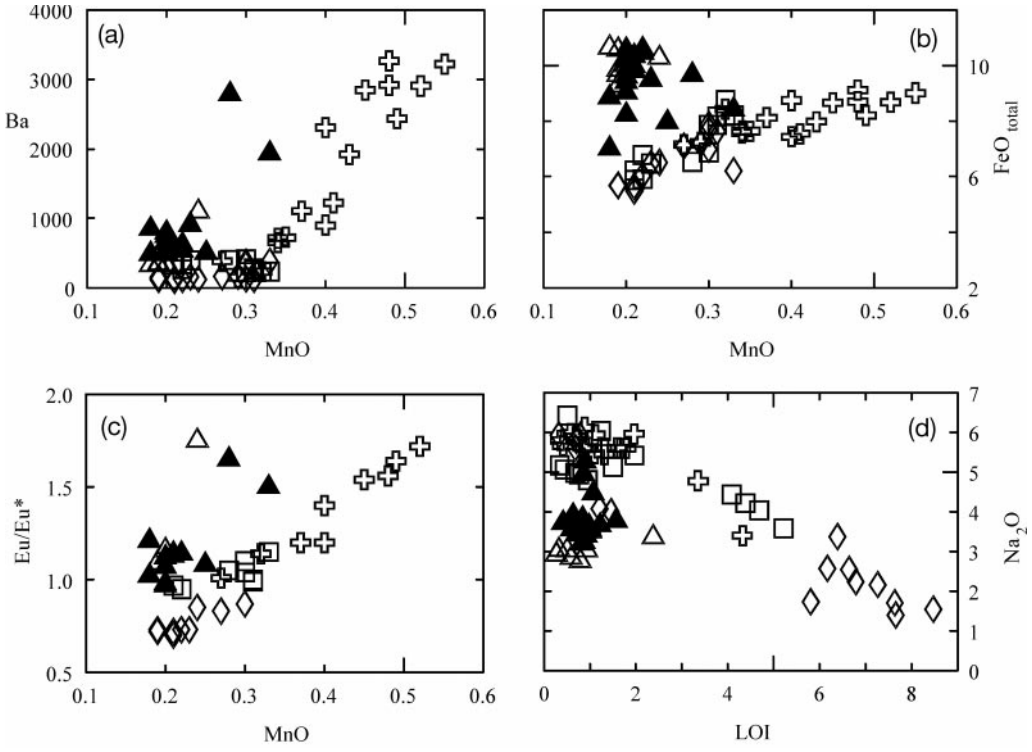

Fig. 10. Variation diagrams of MnO vs Ba, FeO_{total} and Eu/Eu*, and Na_2O vs LOI. Symbols as in Fig. 4.

Crustal melting

Melting of Precambrian crust

Precambrian crust crops out at the margins of the Ethiopian volcanic province, and forms the basement of the Tertiary–Quaternary volcanoes. Major element, trace element and Sr isotopic data on a suite of Precambrian rocks from Sidamo (Southern Ethiopia) (Peccerillo *et al*., 1998) show significant variability. $^{87}Sr/^{86}Sr$ isotope ratios are generally higher than in the Gedemsa rocks (Fig. 7) (Peccerillo *et al*., 1998). Preliminary data indicate that Nd isotopes are lower in the Precambrian rocks, whereas Pb isotopes are comparable with those of the Gedemsa volcanics (Fig. 9). Overall, isotopic evidence (especially Sr and Nd) does not support derivation of Gedemsa rhyolites from Precambrian rock melting.

Ratios of incompatible elements, especially large ion lithophile elements and high field strength elements (LILE/HFSE; e.g. Rb/Nb, Th/Ta, La/Ta, Rb/Zr) are higher in the Precambrian rocks than at Gedemsa (Fig. 7e and f) (see also Ayalew & Peccerillo, 1998; Alene *et al*., 2000). A wealth of studies have shown that melts formed by melting of crustal rocks preserve or increase LILE/HFSE ratios, as LILE are more incompatible than HFSE (Ta, Nb, Zr) during crustal anatexis (e.g. Watt & Harley, 1993; Beard *et al*., 1994; Ayres & Harris, 1997). These distinct trace element ratios, therefore, represent additional evidence against derivation of the Gedemsa silicic rocks by melting of Precambrian basement.

Melting of underplated young basaltic crust

We have tested this hypothesis starting from the compositions of basaltic rocks erupted at Gedemsa as well as other compositions from the Ethiopian rift and plateau (Gasparon *et al*., 1993; Peccerillo *et al*., 1997; Pik *et al*., 1998; Trua *et al*., 1998). Some of the Gedemsa silicic rocks have comparable Sr, Nd and Pb isotope ratios to the basalts, whereas other samples (GD22, GD29, GD34) have higher Sr and slightly lower Nd isotope ratios (Table 4). These data agree with the hypothesis that silicic magmas may be derived through partial melting of basalt, with a contribution from Precambrian crust. Variable isotope compositions have been found in Kenyan peralkaline rocks and have been interpreted as evidence for a contribution from both underplated basalt and old crust (Davies & Macdonald, 1987).

Several workers have suggested that silicic magmas with variable enrichments in alkalis can be generated by melting of basaltic rocks leaving residues dominated by plagioclase and pyroxene (e.g. Thy *et al*., 1990;

Beard & Lofgren, 1991; Garland *et al.*, 1995; Hay & Wendlandt, 1995). To test this hypothesis, we performed equilibrium melting modelling based on simple mass balance calculations for major elements, starting from a rock with a chemical composition like the average Gedemsa basalts and with a gabbroic mineral composition. Mineral compositions like those observed in the Gedemsa basalts were assumed for these rocks. The liquid compositions obtained by about 30% to 10% melting, with residues of plagioclase (about 60%), plus minor amounts of clinopyroxene (about 25%), olivine (10%), magnetite (5%) and apatite (1%), match closely some of the Gedemsa silicic rocks. This supports the idea that an alkaline silicic melt can be obtained by basalt melting, as suggested by several workers.

Partial melting processes have also been tested using incompatible trace elements. Models show that various degrees of batch melting of the Gedemsa basalts generate trends of incompatible elements, such as Rb and Ta (and Nb, Zr, Hf and REE, not shown), that match closely those shown by the Gedemsa trachytes and rhyolites (dashed line in Fig. 11a), assuming low bulk partition coefficients for these elements ($D_{s/l} < 0{\cdot}05$). These values are realistic, as the residual phases inferred from major element modelling, except for accessory apatite, are strongly depleted in incompatible trace elements (see Appendix). Degrees of partial melting around 5% are necessary to match the most enriched liquids, which is not far from the values obtained by major element modelling, considering the uncertainty on the parent rock composition. However, trace element data on clinopyroxenes from the studied basalts (see Appendix), as well as those from the literature (e.g. Drexler *et al.*, 1983; Nielsen, 1990; Mungall & Martin, 1995; Streck & Grunder, 1997), show that this phase has significantly higher partition coefficients for heavy REE (HREE) than for light REE (LREE) ($K_{Lu,Y} = 0{\cdot}8$ and $K_{La} = 0{\cdot}1$ in our rocks; see Appendix). This implies that the presence of 25% clinopyroxene in the residue would make the HREE significantly less incompatible than LREE ($D_{La} < 0{\cdot}1$; $D_{Lu,Y} = 0{\cdot}2$). Therefore, the occurrence of clinopyroxene in the residue should produce a fractionation between LREE and HREE, with generation of liquids displaying significantly higher LREE/HREE ratios than the parent rocks (Fig. 11b, dashed line). However, flat trends for La/Y and La/Lu vs Rb (Fig. 7) are shown by the Gedemsa rocks. It must be noted here that the model trends reported in Fig. 11, and below in the following discussion, change significantly by modifying partition coefficients of solid phases. Therefore, a broadly qualitative significance should be attached to them. The qualitative information emerging from models in Fig. 11 is that batch melting is able to produce linear trends of incompatible elements, but the degrees of enrichments for incompatible elements with different $D_{s/l}$ are variable, and this produces a change in incompatible trace element ratios.

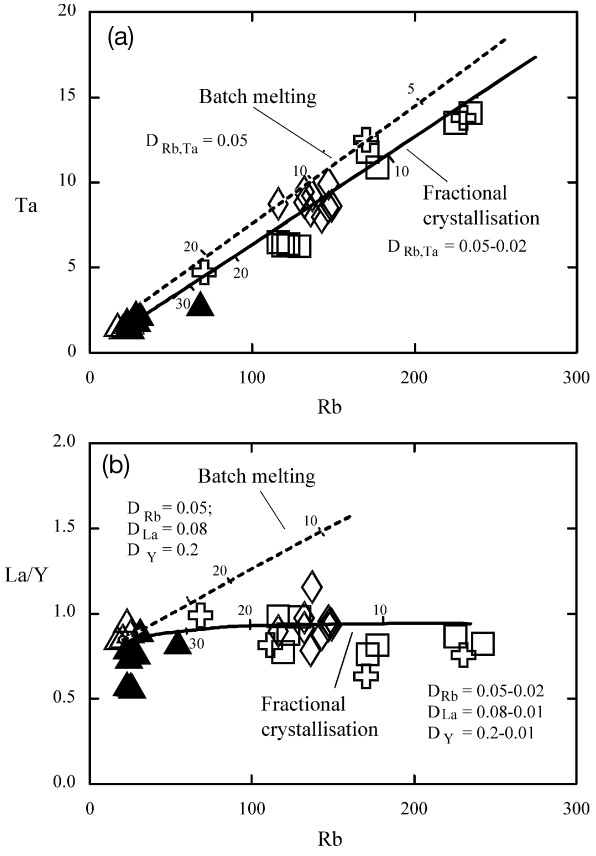

Fig. 11. Rb vs Ta (a) and Rb vs La/Y (b) diagrams for the Gedemsa rocks. Lines are batch melting (dashed line) and fractionation crystallization (continuous line) models starting from the most primitive Gedemsa basalts. Numbers along the lines indicate amount of melt. Bulk partition coefficients ($D_{Rb,La,Y}$) for both batch melting and fractional crystallization have been calculated from major element modelling and using the phenocryst/groundmass concentration ratios reported in the Appendix. Bulk partition coefficients for fractional crystallization are variable, as a result of changes in the fractionating mineral assemblages from mafic magma (dominated by pl + ol + cpx) to salic compositions (dominated by alkali feldspar). (For additional details, see text.) Symbols as in Fig. 4.

Fractional crystallization and AFC

Fractional crystallization processes starting from Gedemsa basalts have been tested for major elements using both mass balance calculations and the thermodynamic modelling of Ghiorso & Sack (1995). Mass balance calculations show that a trachytic composition (such as that of sample GD32) can be reached after about 70% fractional crystallization of Gedemsa

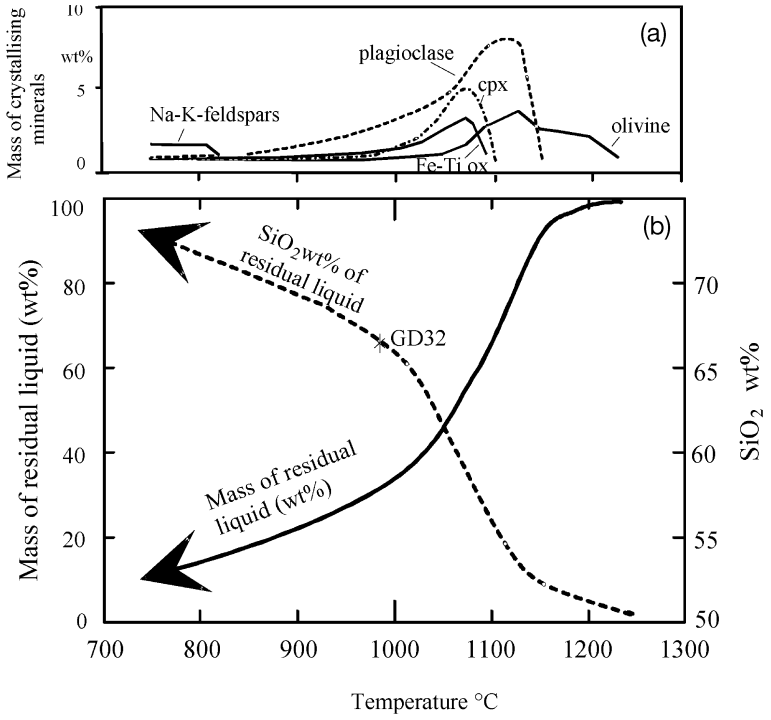

Fig. 12. Thermodynamic modelling of fractional crystallization for the Gedemsa magmas, according to Ghiorso & Sack (1995). (a) Variation of fractionating mass (wt %) of the main minerals with falling temperature. (b) Variation of the mass (wt %) of residual liquid and of its SiO_2 content with falling temperature. (For further explanation, see text.) The composition of the GD32 trachyte is shown on the SiO_2 curve.

basalt, with removal of an assemblage consisting of plagioclase (about 50% of the separating assemblage), olivine (about 20%), clinopyroxene (20%), magnetite (10%) and accessory apatite (1%). Further fractionation (some 50–60%) dominated by separation of alkali feldspar (85–90%) and minor clinopyroxene (around 10%), fayalite (2%) and Fe–Ti oxides (2%) drives residual liquids toward the most silicic composition. Overall, the amount of residual liquid left, after the peralkaline rhyolite composition has been reached, is around 10% of the initial mass of mafic magma. Similar results have been estimated by other workers (e.g. Barberi *et al*., 1975; Caroff *et al*., 1993; Deniel *et al*., 1994; Mungall & Martin, 1995; Civetta *et al*., 1998), but this introduces the problem of where the huge amounts of parental magmas are eventually stored and why the surface evidence of their existence is so weak.

Fractional crystallization has also been modelled using the thermodynamic approach of Ghiorso & Sack (1995), assuming various pressures and oxygen fugacities, and starting from the basaltic samples analysed in this study. The models that better fit the data are those calculated at low pressure (0·05 GPa) and at fO_2 = QFM (quartz–fayalite–magnetite). These conditions agree with oxygen fugacities calculated on ilmenite–haematite pairs for basalts and with the typical low-pressure phenocryst mineralogy of the mafic and silicic rocks under study (e.g. Mahood & Baker, 1986; Caroff *et al*., 1993; Scaillet & Macdonald, 2001, and references therein). A liquid evolution trend, starting from the most primitive basalt, GD65, is shown in the TAS diagram (Fig. 4). These models simply suggest that peralkaline rhyolitic compositions can be reached by low-pressure fractional crystallization, starting from mildly alkaline basalts. The separating phases and the amounts of residual liquid are shown in Fig. 12. Fractionating minerals include early olivine, followed by bytownitic plagioclase; clinopyroxene and magnetite separated at rather advanced stages of fractionation (amount of residual liquid around 60% of the initial mass). Fractional crystallization in the silicic range is dominated by alkali feldspar (more than 80% of the total fractionating assemblage) and by minor alkali pyroxene, fayalite and ilmenite. It should be noted that the amount of residual liquid decreases very sharply during the intermediate stages of fractionation (i.e. at intermediate silica contents), when the various main mineral phases separate contemporaneously from the magma. The amount of residual liquid left after the trachyte composition is reached (GD32, indicated with a tick in Fig. 12) is

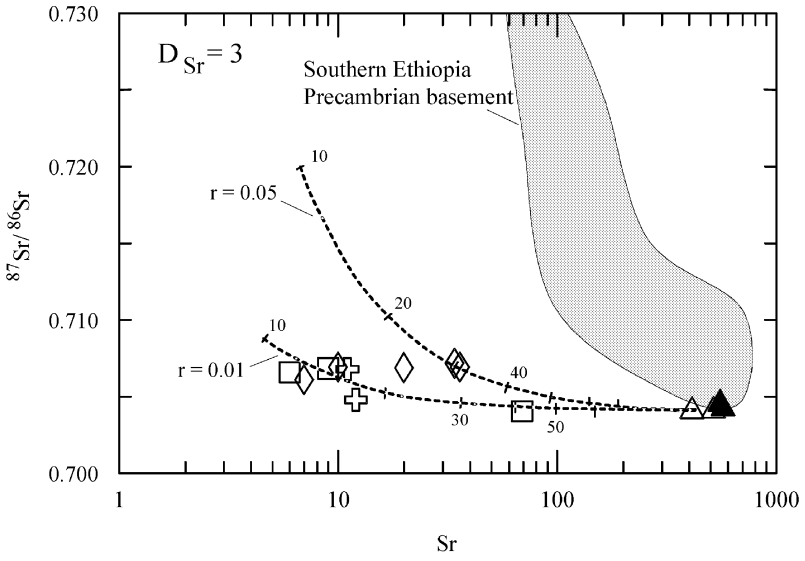

Fig. 13. Sr vs $^{87}Sr/^{86}Sr$ diagram for the Gedemsa rocks. The lines are AFC models (De Paolo, 1981) showing compositional variations of liquids formed from the most primitive basalt, assuming average Precambrian crust (Peccerillo *et al.*, 1998) as assimilant (150 ppm Sr; $^{87}Sr/^{86}Sr = 0{\cdot}731$), bulk partition coefficient $D_{Sr} = 3$, and ratios between masses of assimilated and fractionated material $r = 0{\cdot}05$ and 0·01. Numbers along the lines represent amounts of residual liquids.

about 30% of the initial mass, whereas peralkaline rhyolite composition is reached when about 10% liquid is left. Overall, the low-pressure fractionation model highlights a strong role for olivine and plagioclase separation and minor fractionation of clinopyroxene. Both these results basically agree with mass balance calculations.

A fractional crystallization model based on major elements has been tested using incompatible trace elements, starting from basalt GD65; the results are given in Fig. 11. Bulk partition coefficients have been calculated from major element modelling, using phenocryst/groundmass values reported in the Appendix. They are variable during the course of fractional crystallization, because of the changing fractionating assemblage. Incompatible element abundances of trachytic liquids (represented by the trachytes with no Ba enrichment) can be reached after about 70% fractional crystallization of the most primitive basalt (GD65). Further evolution produces an increase in incompatible elements and, after some 90–95% fractional crystallization, the most evolved compositions are reached. This is basically consistent with the models deduced from major elements. One important aspect of the modelling is that LILE (except Sr and Ba), HFSE and REE (except Eu) are all strongly incompatible for the separating assemblage. This relates to the fact that clinopyroxene fractionates in limited amounts and during a relatively narrow temperature interval (Fig. 12); clinopyroxene discriminates among incompatible elements (e.g. between LREE and HREE), but its moderate separation is insufficient to produce significant incompatible trace element fractionation. It should be noted also that, at constant values of partition coefficients, fractional crystallization is less efficient than partial melting in changing ratios of incompatible trace elements with different degrees of incompatibility (e.g. Hanson, 1978). Therefore, the small variation in incompatible element ratios throughout the entire series of Gedemsa rocks (e.g. La/Lu) is most consistent with fractional crystallization processes.

Variations of radiogenic isotope ratios observed in the Gedemsa rocks require some interaction with crust during evolution. It is unlikely that the radiogenic Sr compositions of the rhyolites are the result of deuteric processes, as high $^{87}Sr/^{86}Sr$ values have been found also in separated feldspar from a rhyolite sample, as mentioned above. Moreover, three samples from the same pumice deposit (GD21, GD22, GD24) gave similar $^{87}Sr/^{86}Sr$ compositions, which argues against significant secondary modification. The range of oxygen isotopic ratios in Gedemsa magmas, as calculated from measured phenocryst compositions (Table 4), is also somewhat higher than expected by simple fractional crystallization (e.g. Anderson *et al.*, 1971; Taylor & Sheppard, 1986). However, AFC modelling (Fig. 13) shows that Sr isotopic compositions like those of the analysed silicic rocks do not require significant interaction with the crust, and a ratio between assimilated and crystallized material much lower than 0·1 is sufficient to match the observed compositions.

In conclusion, data on the Gedemsa volcano fit the hypothesis of a derivation of silicic rocks from mafic

ones by fractional crystallization with a low contribution from the Precambrian crust.

Discriminating between crustal melting and fractional crystallization: the behaviour of compatible elements

Geochemical modelling based on major elements, incompatible trace elements and isotopes does not unambiguously discriminate between basalt melting and basalt fractional crystallization processes in the genesis of Gedemsa peralkaline rhyolites. It is well known that both batch and fractional partial melting processes are able to generate liquids with variable enrichments in incompatible elements, but with moderate depletion in compatible elements; in contrast, fractional crystallization is much more efficient in producing compatible element depletion than incompatible element enrichment (e.g. Hanson, 1978). Therefore, models of incompatible vs compatible trace elements are potentially powerful tools to discriminate between fractional crystallization and melting processes. Variable values of bulk partition coefficients of compatible trace elements make the various elements decrease at different rates during fractional crystallization. For instance, Ni and Cr decrease rapidly during the early stages of basalt fractionation because olivine and Cr-spinel are crystallizing; in contrast, Sr and V remain initially constant or increase slightly, but decrease during intermediate stages of fractionation when plagioclase and Fe–Ti oxides start to crystallize. Sr may behave as compatible or incompatible during melting, depending on the amount of feldspar left in the residue. Therefore, modelling will test various compatible elements, whereas only Zr will be considered among the incompatible elements, as linear positive inter-element trends passing through the origin suggest comparable partition coefficients for all incompatible trace elements.

Geochemical modelling, reported in Fig. 14, shows that the Zr and Sr variations cannot be obtained by a single-stage partial melting of basalts or any other rock, assuming bulk partition coefficients comparable with or even higher than those deduced from melting models of major elements; batch melting processes (dashed curves) produce moderate depletion in Sr at high enrichments in Zr. The compositions of the least evolved trachytes may be reached by partial melting of basalts only if very high values for $D_{Sr} > 5$ are assumed (model not shown). These are unrealistic, unless one assumes that the residue consists almost entirely of plagioclase and the highest values of the partition coefficients for Sr reported in the literature for peralkaline systems are considered (Mahood & Stimac, 1990). In contrast, the overall Sr vs Zr variation in the Gedemsa suite silicic range can be easily

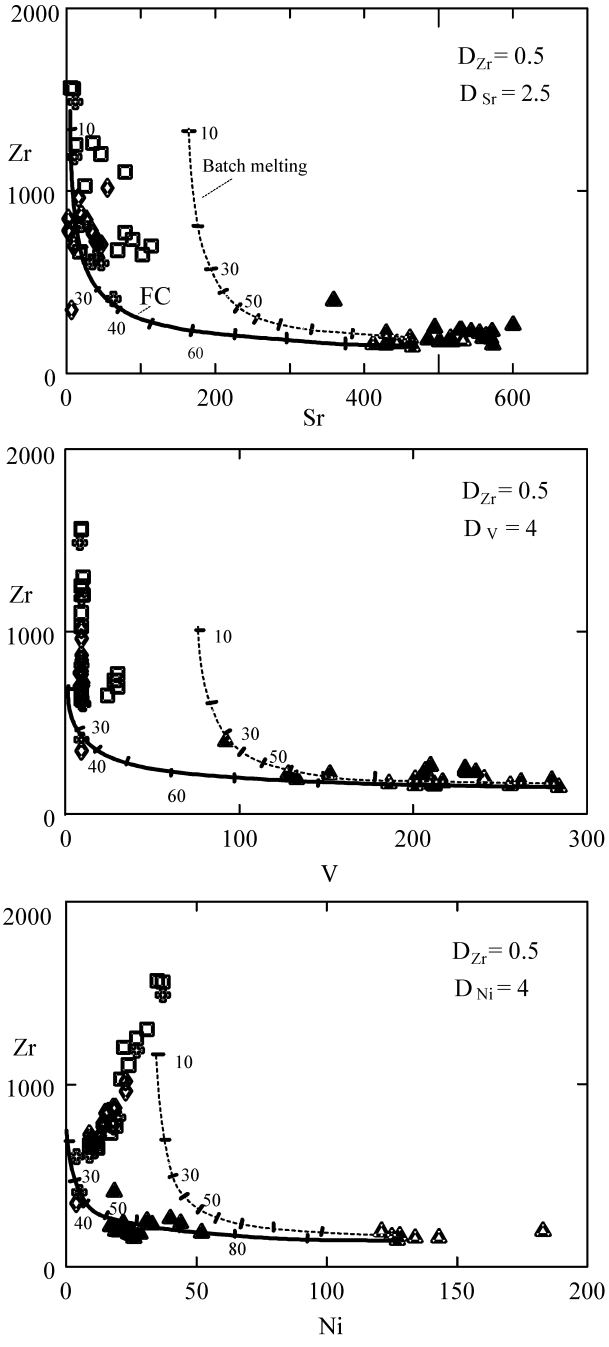

Fig. 14. Variation diagrams with batch melting (dashed line) and fractional crystallization (FC, continuous line) models of compatible vs incompatible trace elements for the Gedemsa rocks. Basalt GD65 has been assumed as the starting composition for both batch melting and fractional crystallization. Partition coefficients are average values estimated from major element modelling and from values of mineral/groundmass reported in the Appendix. Symbols as in Fig. 4.

obtained by fractional crystallization starting from basalt, assuming a compatible behaviour for Sr (D_{Sr} = 2–3); these values of partition coefficients are somewhat higher than those of mafic systems, but are close

to those of silicic magmas in which feldspar is the dominant fractionating phase. Starting from basalt GD65, the composition of the least evolved trachyte is reached after about 70% fractional crystallization, in agreement with models based on major elements and incompatible trace elements (Figs 11 and 12). The low contents of Ni and V in the trachytes cannot be explained by single-stage partial melting of basalt unless extremely high and very unrealistic values of partition coefficients are assumed for the residual solid ($D_{s/l}$ up to 50; model not shown); in contrast, these are readily explained by fractional crystallization, assuming values of partition coefficients consistent with major element modelling ($D_{s/l} = 3$–4). It should be noted that the smooth linear positive correlation of Ni with Zr in the silicic rocks requires that this element exhibited an incompatible behaviour in the silicic compositions, in agreement with the hypothesis that fractionation was dominated by feldspar with small amounts of mafic phases. It should be noted also that some of the post-caldera rhyolites plot to the right of the fractional crystallization curves. This probably denotes small degrees of mixing with mafic magmas for some post-caldera rhyolites. In contrast, most enclaves plot on the fractional crystallization curve.

Therefore, compatible vs incompatible element modelling clearly suggests that partial melting cannot be responsible for the genesis of the rhyolitic rocks. Also, the trachytes have exceedingly low concentrations of compatible elements, which are difficult to model by basalt melting. Therefore, an overall derivation from basalts by fractional crystallization is favoured by geochemical models of compatible vs incompatible elements.

It could be argued, however, that trachytes are not derived from basalts but from slightly more evolved rocks. In other words, the basalts may have first undergone fractionation that generated evolved magmas depleted in compatible elements; these solidified and subsequently underwent partial melting to give silicic magmas. However, there is some objection to this hypothesis. First, a two-stage model works well only for those elements (e.g. Co, Ni, Cr) that are compatible in the early stages of fractionation. The problem becomes more complicated for those elements, such as Sr and V, that behave as moderately incompatible during early to intermediate stages of fractionation and remain constant or increase from basalts to intermediate magmas. For example, data on mafic to intermediate rocks (SiO_2 ranging from 45 to 55 wt %) from the Ethiopian rift and plateau show that Sr and V have invariably high values, with Sr $>$ 200–300 ppm, and V $>$ 100 ppm and mostly in the range 200–400 ppm (Hart *et al.*, 1989; Gasparon *et al.*, 1993; Peccerillo *et al.*, 1997; Pik *et al.*, 1998; Barberio *et al.*, 1999). Therefore, the difficulty of modelling the low concentrations of Sr and V in the Gedemsa silicic rocks remains, even if intermediate magmas are assumed as starting compositions. Moreover, the assumption of a two-stage model does not explain the lack or scarcity of intermediate rocks and, therefore, does not offer a satisfactory explanation for the Daly Gap, which remains one of the most appealing lines of evidence in favour of the basalt melting hypothesis.

Further support for the fractional crystallization hypothesis arises from a comparison between the Gedemsa volcanics and the suite from the Boina centre, Afar. Here, silicic peralkaline rocks are found associated with abundant transitional basalts and there is general agreement that the entire suite was generated by fractional crystallization (Barberi *et al.*, 1975; Macdonald *et al.*, 1987; Scaillet & Macdonald, 2001). The Boina rhyolites have very similar compositions to rhyolites from Gedemsa, for both major and many trace elements. Moreover, element trends within the Boina suite very closely match those observed at Gedemsa (see Figs 4–7). The main difference between the two volcanoes is in the relative abundance of the various magma types: silicic rocks prevail at Gedemsa, whereas basalts dominate at Boina. We believe that although the close matching of compositional variations reveals the same type of genesis, the variable amounts of magma types depend on the structure of the plumbing systems of the two volcanoes. It should be noted that Gedemsa is characterized by a large central caldera, which reveals a shallow-level magma chamber.

The 'Daly Gap' problem and models for the volcanic plumbing system at Gedemsa

Geochemical data suggest that fractional crystallization of basalt, with minor assimilation of Precambrian crust, provides the most satisfactory explanation for the geochemistry of the silicic rocks at Gedemsa. However, as fractionation of basalts produces a continuum of compositions, the problem of the absence or scarcity of intermediate rocks (Daly Gap) requires an explanation. Also, the predominance of silicic (daughter) with respect to mafic (parental) magmas is a serious problem. Several hypotheses have been proposed by various workers to explain these observations. Classical models of magma chambers (Turner & Campbell, 1986) suggest that crystallization along walls generates lighter, silica-rich liquids, which migrate toward the top of the reservoir; here they accumulate and possibly undergo further evolution. Mafic magma ponding at the bottom of the chamber is subjected to continuous

stirring and mixing with newly injected mafic melts, which prevent evolution toward silicic compositions. The upper silicic layer acts as a density barrier with respect to the underlying mafic magma, which is prohibited from reaching the surface. As a result, silicic magmas with variable degrees of evolution are preferentially erupted, whereas the mafic magmas are tapped sporadically, possibly only when the upper part of the reservoir is completely emptied. Other models (e.g. Marsh, 1981; Brophy, 1991) suggest that large phenocryst loads prevent convective stirring, thus forming stratified magma chambers.

Thermodynamic modelling reported in this study shows that the mass of residual liquids during fractional crystallization from basalt to rhyolite does not change linearly with falling temperature, but decreases slowly during early and late stages, and drops abruptly at intermediate degrees of fractional crystallization (Fig. 12). When the mass of residual liquid and the calculated silica content of the residual magmas are considered, it is observed that a sharp decrease of mass coincides with intermediate compositions. These data suggest that, with a steady fall in temperature, fractionating magmas pass rapidly through the intermediate stages, i.e. producing relatively small amounts of intermediate melts. This is expected, as contemporaneous separation of various minerals occurs over a narrow temperature interval (Clague, 1978). Therefore, the mechanism of fractional crystallization effectively reduces the volume of intermediate melts. Moreover, the calculated densities of the Gedemsa magmas suggest values of about 2700 kg/m^3 for mafic melts, 2400–2600 kg/m^3 for intermediate magmas and lower than 2400 kg/m^3 for silicic melts. This means that in a fractionating, continuously fed magma chamber, the silicic melts will occupy the top of the reservoir and the mafic magmas pond at the bottom, whereas minor intermediate melts, rich in crystals, form the interface between the two zones (Wolff & Storey, 1984; Turner & Campbell, 1986). These can be easily dragged upward by silicic melts and brought to the surface as enclaves when eruptions tap the intermediate levels of the zoned magma chamber.

The pre-caldera lavas and pyroclastic rocks at Gedemsa have rather homogeneous compositions, without any trace of mingling with mafic melt. Mingling between magmas with different compositions appears during the syn-caldera ignimbrite eruption and becomes a prominent feature of the post-caldera activity. The porphyritic nature of the mafic and intermediate inclusions occurring in the post-caldera rhyolites and the lack of skeletal crystals suggest slow cooling and a long residence time within the reservoir, where they are derived from basalts by fractional crystallization. This is supported by the curved trends described by most enclaves on compatible vs incompatible element plots.

These lines of evidence support a model in which pre-caldera eruptions tap the top of a magma chamber that is zoned and continuously fractionating and refilling. During the syn- and post-caldera stages, possibly as a result of a reduction in the size of the magma chamber, the intermediate and mafic magmas lying in the middle part of the chamber were tapped and erupted intermingled with silicic melts. Therefore, the Daly Gap at Gedemsa results from two concurrent factors, i.e. the scarcity of intermediate magmas generated by fractionation processes and the stratification of the magma chamber.

The late basalts erupted along the Wonji fault probably represent an independent episode of magmatism, which probably reflects basalt upwelling on a regional scale along extensional fractures parallel to the rift margins (Wonji Fault System). The presence of mingled silicic material in the Wonji Basalts erupted inside the caldera suggests that, during the waning stages of Gedemsa activity, this new pulse of mafic magmas coming from depth cut through the Gedemsa magma chamber, entraining some silicic liquids and partially crystallized rocks.

Implications for regional evolution of volcanism

A crucial requirement of the model presented above is that there was a large magma chamber beneath Gedemsa. This is in agreement with the occurrence of a wide caldera. Large caldera depressions are widespread along the floor of the northern Ethiopian rift. More than 10 caldera collapses can be identified on the basis of satellite images over a rift sector shorter than 100 km, from Gedemsa to the southwestern margin of the Afar. In some sectors (e.g. Kone volcano, about 80 km NE of Gedemsa) several nested collapses are recognizable, one with a diameter of the order of tens of kilometres. Most of these calderas are cut by recent Wonji faults and are extensively covered by younger volcanic activity; therefore, their number is possibly underestimated.

Regional gravity studies (Mahatsente *et al.*, 1999; T. Korme, personal communication, 2002) have revealed several positive anomalies along the floor of the northern Ethiopian rift. These have circular shapes and display a patchy areal distribution (see fig. 4 of Mahatsente *et al.*, 1999). Notably, many of these positive anomalies coincide with rhyolitic volcanoes, and one has been detected beneath Gedemsa. According to Mahatsente *et al.* (1999), these anomalies represent the surface expression of intrusive bodies occurring beneath the volcanoes. Three-dimensional modelling of the gravimetric data has identified various

intrusions along the rift, with an inferred density of 3000–3100 kg/m^3; in most bodies, there is a density decrease from bottom to top. The intrusions are rooted in the mantle and their tops reach a depth of 20 km to less than 4 km. A shallow intrusion was detected beneath Gedemsa (figs 8 and 9 of Mahatsente *et al.*, 1999). According to Mahatsente *et al.*, the high-density bodies represent mantle intrusions within the rift crust. The density zoning from bottom to top was interpreted as due to some interaction between mantle and crustal material. We believe it unlikely that dense upper-mantle material has intruded the crust, reaching depths as shallow as 4 km. Instead, we suggest that the high-density bodies recognized by analysis of gravimetric data represent crystallized magmatic material, basically consisting of mafic magmas and their cumulates. The match between circular gravity anomalies and silicic centres supports the hypothesis that large silicic central volcanoes developed above large intrusions of mafic magmas; these underwent fractional crystallization and moderate crustal assimilation. The silicic material sitting at the top of the chambers was preferentially erupted, whereas mafic material was left at depth. The crystallization of these magmas gave rise to mafic rocks and mafic to ultramafic cumulates, which are revealed by gravimetric measurements.

In conclusion, geophysical evidence suggests that the petrological and volcanological models proposed for Gedemsa may be of wider applicability for the Ethiopian rift valley and may represent an explanation for the large prevalence of silicic rocks on a regional scale.

CONCLUSIONS

Petrological and geochemical data on volcanic rocks from Gedemsa volcano preclude models in which silicic magmas are derived by partial melting of Precambrian crust or by a single-stage melting of young mafic rocks. The process that best explains the geochemical and petrological variations at Gedemsa is a continuous fractional crystallization of transitional basaltic magmas, with moderate assimilation of Precambrian crust.

It is suggested that mafic magmas evolving in a shallow-level, zoned, magma chamber produced silica-rich liquids. Early eruptions tapped the upper part of the chamber, allowing the silicic melts to reach the surface. The basic and intermediate magmas ponding below the silicic cap were tapped after the caldera collapse, when the size of the reservoir was considerably reduced, and reached the surface intensively intermingled with silicic melts.

The scarcity or absence of intermediate magmas is believed to derive essentially from the narrow temperature interval over which intermediate melts formed, a process that significantly reduces the amount of intermediate magmas.

The Gedemsa volcano sits over a zone of positive gravity anomaly, which suggests the presence of a high-density intrusive body, most probably represented by mafic and ultramafic cumulate rocks. There is a patchy distribution of circular positive gravity anomalies along the Ethiopian rift floor, most of which coincide with silicic volcanoes. This supports the hypothesis that several magma chambers formed along the rift floor. These were internally zoned, and their silicic upper part was preferentially tapped by eruptions, thus explaining the large prevalence of rhyolitic rocks along the Ethiopian rift.

ACKNOWLEDGEMENTS

The work on the Gedemsa volcano and on the Ethiopian rift was funded by the Italian Ministry of Education, University and Research (MIUR). Most of the knowledge on Ethiopian volcanism, which served as a basis for the present work, was acquired while the senior author (A.P.) was working at the Department of Geology and Geophysics of the Addis Ababa University, in the frame of the technical co-operation between the Ministry of Foreign Affairs of Italy and the Addis Ababa University. The authors express their thanks to Wendy Bohrson and Anita Grunder for stimulating and constructive reviews. Many thanks go to Keith Bell, Carleton University of Ottawa, for determining Pb isotopic compositions, and to Enzo Pagana and Danilo Chiocchini, University of Perugia, for wet chemistry and X-ray fluorescence analyses.

REFERENCES

Alene, M., Ruffini, R. & Sacchi, R. (2000). Geochemistry and geotectonic setting of Neoproterozoic rocks from Northern Ethiopia (Arabian–Nubian Shield). *Gondwana Research* **3**, 333–347.

Anderson, A. T., Clayton, R. N. & Mayeda, T. K. (1971). Oxygen isotope thermometry of mafic igneous rocks. *Journal of Geology* **79**, 715–729.

Appora, I., Eiler, J. M., Matthews, A. & Stolper, E. M. (2003). Experimental determination of oxygen isotope fractionation between CO_2 vapor and soda–melilite melt. *Geochimica et Cosmochimica Acta* **67**, 459–471.

Ayalew, T. & Peccerillo, A. (1998). Petrology and geochemistry of the Gore Gambella plutonic rocks: implications for magma genesis and the tectonic setting of the Pan-African Orogenic Belt of western Ethiopia. *Journal of African Earth Sciences* **27**, 397–416.

Ayalew, D., Yirgu, G. & Pik, R. (1999). Geochemical and isotopic (Sr, Nd and Pb) characteristics of volcanic rocks from southwestern Ethiopia. *Journal of African Earth Sciences* **29**, 381–391.

Ayres, M. & Harris, N. (1997). REE fractionation and Nd-isotope disequilibrium during crustal anatexis: constraints from Himalayan leucogranites. *Chemical Geology* **139**, 249–269.

Barberi, F., Ferrara, G., Santacroce, R., Treuil, M. & Varet, J. (1975). A transitional basalt–pantellerite sequence of fractional crystallisation, the Boina centre (Afar Rift, Ethiopia). *Journal of Petrology* **16**, 22–56.

Barberio, M. R., Donati, C., Donato, P., Yirgu, G., Peccerillo, A. & Wu, T. W. (1999). Petrology and geochemistry of Quaternary magmatism in the northern sector of the Ethiopian Rift between Debre Zeit and Awash Park. *Acta Vulcanologica* **11**, 69–81.

Beard, J. S. & Lofgren, G. E. (1991). Dehydration melting and water-saturated melting of basaltic and andesitic greenstones and amphibolites at 1, 3, and 6·9 kbar. *Journal of Petrology* **32**, 365–401.

Beard, J. S., Lofgren, G. E., Sinha, K. & Tollo, R. P. (1994). Partial melting of apatite-bearing charnockite, granulite, and diorite: melt compositions, restite mineralogy, and petrologic implications. *Journal of Geophysical Research* **99**, 21591–21603.

Bell, K. & Tilton, G. R. (2001). Nd, Pb and Sr isotopic compositions of East African carbonatites: evidence for mantle mixing and plume inhomogeneity. *Journal of Petrology* **42**, 1927–1945.

Bellieni, G., Comin Chiaramonti, P., Marques, L. S., Melfi, A. J., Nardy, A. J. R., Papatrechas, C., Piccirillo, E. M., Roisenberg, A. & Stolfa, D. (1985). Petrogenetic aspects of acid and basaltic lavas from the Paranà Plateau (Brazil): geological, mineralogical and petrochemical relationships. *Journal of Petrology* **27**, 915–944.

Berhe, S. M., Desta, B., Nicoletti, C. & Teferra, M. (1987). Geology, geochronology and geodynamic implications of the Cenozoic magmatic province in W and SE Ethiopia. *Journal of the Geological Society, London* **144**, 213–226.

Black, S., Macdonald, R. & Kelly, M. R. (1997). Crustal origin of peralkaline rhyolites from Kenya: evidence from U-series disequilibria and Th-isotopes. *Journal of Petrology* **38**, 277–297.

Bohrson, W. A. & Reid, M. R. (1997). Genesis of peralkaline volcanic rocks in an ocean island setting by crustal melting and open-system processes: Socorro Island, Mexico. *Journal of Petrology* **38**, 1137–1166.

Bonnefoi, C. C., Provost, A. & Albarede, F. (1999). Thermochemical dynamics of magma chambers: a simple model. *Journal of Geophysical Research* **104**, 7103–7115.

Brophy, J. G. (1991). Compositional gaps, critical crystallinity and fractional crystallisation in orogenic (calc-alkaline) magmatic systems. *Contributions to Mineralogy and Petrology* **109**, 173–182.

Campbell, I. H. & Griffiths, R. W. (1992). The changing nature of hotspots through time: implications for the chemical evolution of the mantle. *Journal of Geology* **92**, 497–523.

Caroff, M., Maury, R. C., Leterrier, J., Joron, J. L. & Cotten, J. (1993). Trace element behavior in the alkalic basalt comenditic trachyte series from Mururoa atoll, French Polynesia. *Lithos* **30**, 1–22.

Chazot, C. & Bertrand, H. (1995). Genesis of silicic magmas during Tertiary continental rifting in Yemen. *Lithos* **36**, 69–83.

Cioni, R., Cristiani, C., De Rosa, R., Marianelli, P., Mazzuoli, R., Ayalew, D., Yirgu, G. & Bompressi, E. (2001). Trachyte–pantellerite syn-eruptive magma mixing: evidence from the caldera-forming ignimbrite at Gedemsa (Main Ethiopian Rift). In: *GEOITALIA 2001, 3rd Earth Science Forum, Abstract Volume*. Chieti: Federazione Italiana Scienze della Terra, pp. 711–712.

Civetta, L., D'Antonio, M., Orsi, G. & Tilton, G. R. (1998). The geochemistry of volcanic rocks from Pantelleria island, Sicily Channel: petrogenesis and characteristics of the mantle source region. *Journal of Petrology* **39**, 1453–1491.

Clague, D. A. (1978). The oceanic basalt–trachyte association: an explanation of the Daly Gap. *Journal of Geology* **86**, 739–743.

Cotten, J., Le Dez, A., Bau, M., Caroff, M., Maury, R. C., Dulski, P., Fourcade, S., Bohn, M. & Brousse, R. (1995). Origin of anomalous rare-earth element and yttrium enrichments in subaerially exposed basalts: evidence from French Polynesia. *Chemical Geology* **119**, 115–138.

Davies, G. F. (1998). Plate, plumes, mantle convection, and mantle evolution. In: Jackson, I. (ed.) *The Earth's Mantle*. Cambridge: Cambridge University Press, pp. 228–258.

Davies, J. R. & Macdonald, R. (1987). Crustal influence in the petrogenesis of the Naivasha basalt–comendite complex: combined trace element and Sr–Nd–Pb isotope constraints. *Journal of Petrology* **28**, 1009–1031.

Deniel, C., Vidal, P., Coulon, C., Vellutini, P. J. & Piguet, P. (1994). Temporal evolution of mantle source during continental rifting: the volcanism of Djibouti (Afar). *Journal of Geophysical Research* **99**, 2853–2869.

De Paolo, D. J. (1981). Trace element and isotopic effects of combined wall rock assimilation and fractional crystallization. *Earth and Planetary Science Letters* **53**, 189–202.

Di Paola, G. M. (1972). The Ethiopian Rift Valley (between 7·00′ and 8·40′ lat. North). *Bulletin of Volcanology* **36**, 317–560.

Drexler, J. W., Bornhorst, T. J. & Noble, D. C. (1983). Trace element sanidine/glass distribution coefficients for peralkaline silicic rocks and their implications to peralkaline petrogenesis. *Lithos* **16**, 265–271.

Garland, F., Hawkesworth, C. J. & Mantovani, M. S. M. (1995). Description and petrogenesis of the Paranà rhyolites. *Journal of Petrology* **36**, 1193–1227.

Gasparon, M., Innocenti, F., Manetti, P., Peccerillo, A. & Tsegaye, A. (1993). Genesis of the Pliocene to Recent bimodal mafic–felsic volcanism in the Debre Zeit area, Central Ethiopia: volcanological and geochemical constraints. *Journal of African Earth Sciences* **17**, 145–165.

Geist, D., Howard, K. A. & Larson, P. (1995). The generation of oceanic rhyolites by crystal fractionation: the basalt–rhyolite association at Volcàn Alcedo, Galapagos Archipelago. *Journal of Petrology* **36**, 965–982.

Ghiorso, M. S. & Sack, R. O. (1995). Chemical transfer in magmatic processes: IV. A revised and internally consistent thermodynamic model for the interpolation and extrapolation of liquid–solid equilibria in magmatic system at elevated temperatures and pressures. *Contributions to Mineralogy and Petrology* **119**, 197–212.

Hanson, G. N. (1978). The application of trace elements to the petrogenesis of igneous rocks of granitic composition. *Earth and Planetary Science Letters* **38**, 26–43.

Hart, W. K., WoldeGabriel, G., Walter, R. C. & Mertzman, S. A. (1989). Basaltic volcanism in Ethiopia: constraints on continental rifting and mantle interaction. *Journal of Geophysical Research* **94**, 7731–7748.

Hay, E. D. & Wendlandt, R. F. (1995). The origin of Kenya rift plateau-type phonolites: results of high-pressure/high-temperature experiments in the system phonolite–H_2O and phonolite–H_2O–CO_2. *Journal of Geophysical Research* **100**, 401–410.

Hofmann, C., Courtillot, V., Féraud, G., Rochette, P., Yrgu, G., Ketefo, E. & Pik, R. (1997). Timing of the Ethiopian flood basalts event and implications for plume birth and global change. *Nature* **389**, 838–841.

Kazmin, V., Berhe, S. M., Nicoletti, M. & Petrucciani, C. (1980). Evolution of the northern part of the Ethiopian Rift. *Rendiconti dell'Accademia Nazionale dei Lincei* **47**, 275–292.

Le Bas, M. J., Le Maitre, R. W., Streckeisen, A. & Zanettin, B. (1986). A chemical classification of volcanic rocks based on the total alkali–silica diagram. *Journal of Petrology* **27**, 745–750.

Lightfoot, P. C., Hawkesworth, C. J. & Setnha, S. F. (1987). Petrogenesis of rhyolites and trachytes from the Deccan Trap: Sr, Nd and Pb isotope and trace element evidence. *Contributions to Mineralogy and Petrology* **95**, 44–54.

Lowenstern, J. B. & Mahood, G. A. (1991). New data on magmatic H_2O contents of pantellerites, with implications for petrogenesis and eruptive dynamics at Pantelleria. *Bulletin of Volcanology* **54**, 78–83.

Macdonald, R. (1974). Nomenclature and petrochemistry of the peralkaline oversaturated extrusive rocks. *Bulletin of Volcanology* **38**, 498–516.

Macdonald, R., Davies, G. R., Bliss, C. M., Leat, P. T., Bailey, D. K. & Smith, R. L. (1987). Geochemistry of high-silica rhyolites, Naivasha, Kenya rift valley. *Journal of Petrology* **28**, 979–1088.

Macdonald, R., Rogers, N. W., Fitton, J. G., Black, S. & Smith, M. (2001). Plume–lithosphere interactions in the generation of the basalts of the Kenya rift, East Africa. *Journal of Petrology* **42**, 877–900.

Mahatsente, R., Jentzsch, G. & Jahr, T. (1999). Crustal structure of the Main Ethiopian Rift from gravity data: 3-dimensional modeling. *Tectonophysics* **313**, 363–382.

Mahood, G. A. & Baker, D. R. (1986). Experimental constraints on depth of fractionation of mildly alkalic basalts and associated felsic rocks: Pantelleria, Strait of Sicily. *Contributions to Mineralogy and Petrology* **93**, 251–264.

Mahood, G. A. & Stimac, J. A. (1990). Trace-element partitioning in pantellerites and trachytes. *Geochimica et Cosmochimica Acta* **54**, 2257–2276.

Mahood, G. A., Halliday, A. N. & Hildreth, W. (1990). Isotopic evidence for the origin of pantellerites in a rift-related alkalic suite: Pantelleria, Italy. In: *IAVCEI Abstracts, International Volcanological Congress*. Mainz.

Marsh, B. D. (1981). On the crystallinity, probability of occurrence, and rheology of lava and magma. *Contributions to Mineralogy and Petrology* **78**, 85–98.

Marty, B., Pik, R. & Yirgu, G. (1996). Helium isotopic variations in Ethiopian plume lavas: nature of magmatic sources and limit on lower mantle contribution. *Earth and Planetary Science Letters* **144**, 223–237.

Merla, G., Abatte, E., Azzaroli, A., Bruni, P., Fazzuoli, M., Sagri, M. & Tacconi, P. (1979). *Comments and a Geological Map of Ethiopia and Somalia. Scale 1:2,000,000*. Florence: Consiglio Nazionale delle Ricerche, 89 pp.

Mohr, P. A. (1967). The Ethiopian Rift System. *Bulletin of the Geophysical Observatory, Addis Ababa* **11**, 1–65.

Mohr, P. A. (1971). Ethiopian rift and plateaus: some volcanic and petrochemical differences. *Journal of Geophysical Research* **76**, 1967–1983.

Mohr, P. A. & Zanettin, B. (1988). The Ethiopian flood basalt province. In: Macdougall, J. D. (ed.) *Continental Flood Basalts*. Dordrecht: Kluwer Academic, pp. 63–110.

Mungall, J. E. (2002). Empirical models relating viscosity and trace diffusion in magmatic silicate melts. *Geochimica et Cosmochimica Acta* **66**, 125–143.

Mungall, J. E. & Martin, R. F. (1995). Petrogenesis of basalt–comendite and basalt–pantellerite suites, Terceira, Azores, and some implications for the origin of oceanic rhyolites. *Contributions to Mineralogy and Petrology* **119**, 43–55.

Nakamura, N. (1974). Determination of REE, Ba, Fe, Mg, Na and K in carbonaceous and ordinary chondrites. *Geochimica et Cosmochimica Acta* **38**, 757–775.

Nakamura, E. & Kushiro, I. (1998). Trace element diffusion in jadeite and diopside melts at high pressures and its geochemical implication. *Geochimica et Cosmochimica Acta* **62**, 3151–3160.

Nielsen, R. L. (1990). Simulation of igneous differentiation processes. In: Nicholls, J. & Russell, J. K. (eds) *Modern Methods of Igneous Petrology: Understanding Magmatic Processes. Mineralogical Society of America, Reviews in Mineralogy* **24**, 65–106.

Peccerillo, A., Gezahegn, Y., Bekele, M. & Wu, T. W. (1997). Fractional crystallization, magma mixing and crustal assimilation in the evolution of plateau and rift magmatism in Ethiopia. In: Li, Z. (ed.) *Proceedings 30th International Geological Congress, Beijing 4–13 August 1996*. Utrecht: VPS International Science Publishers, pp. 137–152.

Peccerillo, A., Mandefro, B., Solomon, G., Hambisa, G., Beru, H. & Tesfaye, K. (1998). The Precambrian rocks from Southern Ethiopia: petrology, geochemistry and their interaction with the recent volcanism from the Ethiopian Rift Valley. *Neues Jahrbuch für Minereralogie, Abhandlungen* **173**, 237–262.

Piccirillo, E. M., Justin-Visentin, E., Zanettin, B., Joron, J. K. & Treuil, M. (1979). Geodynamic evolution from plateau to rift: major and trace element geochemistry of the central eastern Ethiopian plateau volcanics. *Neues Jahrbuch für Geologie und Palaontologie* **258**, 139–179.

Pik, R., Deniel, C., Coulon, C., Yirgu, G., Ayalew, D. & Legros, P. (1998). The northwestern Ethiopian plateau basalts: classification and spatial distribution of magma types. *Journal of Volcanology and Geothermal Research* **81**, 91–111.

Pik, R., Deniel, C., Coulon, C., Yirgu, G. & Marty, B. (1999). Isotopic and trace element signatures of Ethiopian flood basalts: evidence for plume–lithosphere interaction. *Geochimica et Cosmochimica Acta* **63**, 2263–2279.

Rogers, N. W., Macdonald, R., Fitton, J. G., George, R. M., Smith, M. & Barreiro, B. A. (2000). Two mantle plumes beneath the East Africa rift system: Sr, Nd and Pb isotope evidence from Kenya Rift basalts. *Earth and Planetary Science Letters* **176**, 387–400.

Scaillet, B. & Macdonald, R. (2001). Phase relations of peralkaline silicic magmas and petrogenetic implications. *Journal of Petrology* **42**, 825–845.

Streck, M. J. & Grunder, A. L. (1997). Compositional gradients and gaps in high-silica rhyolites of the Rattlesnake tuff, Oregon. *Journal of Petrology* **38**, 133–163.

Taylor, H. P. & Sheppard, S. M. F. (1986). Igneous rocks. I: Processes of isotopic fractionation and isotope systematics. In: Valley, J. W., Taylor, H. P., Jr & O'Neil, J. R. (eds) *Stable Isotopes in High Temperature Geological Processes. Mineralogical Society of America, Reviews in Mineralogy* **16**, 227–272.

Thrall, R. (1973). Gedemsa caldera, Ethiopia. *Center for Astrophysics, Dartmouth College, USA, Reprint Series* **280**, 71–80.

Thy, P., Beard, J. S. & Logfren, G. E. (1990). Experimental constraints on the origin of Icelandic rhyolites. *Journal of Geology* **98**, 417–421.

Todt, W., Cliff, R. A., Houser, A. & Hofmann, A. W. (1995). Evaluation of a 202Pb–205Pb double spike for high precision analyses. In: Basu, A. & Hart, S. (eds) *Earth Processes: Reading the Isotope Code. Geophysical Monograph, American Geophysical Union* **95**, 429–437.

Trua, T., Deniel, C. & Mazzuoli, R. (1998). Crustal control in the genesis of Plio-Quaternary bimodal magmatism of the Main Ethiopian Rift (MER): geochemical and isotopic (Sr Nd, Pb) evidence. *Chemical Geology* **155**, 201–231.

Turner, J. S. & Campbell, I. H. (1986). Convection and mixing in magma chambers. *Earth-Science Reviews* **23**, 255–352.

Watt, G. R. & Harley, S. L. (1993). Accessory phase controls on the geochemistry of crustal melts and restites produced during water undersaturated partial melting. *Contributions to Mineralogy and Petrology* **101**, 220–231.

White, R. S. & McKenzie, D. (1989). Magmatism at rift zones: the generation of volcanic continental margins and flood basalts. *Journal of Geophysical Research* **94**, 7685–7729.

Wolff, J. A. & Storey, M. (1984). Zoning in highly alkaline magma bodies. *Geological Magazine* **121**, 563–575.

Yemane, T., WoldeGabriel, G., Tesfaye, S., Berhe, S. M., Durary, S., Ebinger, C. & Kelley, S. (1999). Temporal and geochemical characteristics of Tertiary volcanic rocks and tectonic history in the southern Main Ethiopian Rift and adjacent volcanic fields. *Acta Vulcanologica* **11**, 99–120.

Yirgu, G., Dereje, A., Peccerillo, A., Barberio, M. R., Donati, C. & Donato, P. (1999). Fluorine and chlorine distribution in the volcanic rocks from the Gedemsa volcano, Ethiopian Rift Valley. *Acta Vulcanologica* **11**, 169–176.

APPENDIX: MINERAL/GROUNDMASS ELEMENT CONCENTRATION RATIOS MEASURED ON GEDEMSA ROCKS AND USED AS PARTITION COEFFICIENTS IN GEOCHEMICAL MODELLING

Element	Olivine (GD65)	Pyroxene (GD65)	Plagioclase (GD65)	Alkali feldspar (GD4)	Magnetite (GD26)
Rb	0·04	0·05	0·05	0·29	0
Ba	0·01	0·03	0·43	3·43	0·01
Sr	0·02	0·09	2·53	2·79	0·1
Zr	0·01	0·17	0·02	<0·01	0·2
Nb–Ta	0·01	0·2	0·01	<0·01	—
La	0·01	0·11	0·12	0·01	—
Sm	0·01	0·49	0·05	0·01	—
Eu	0·01	0·36	0·34	0·52	—
Lu	0·03	0·75	0·02	<0·01	—
Y	0·02	0·8	0·03	0·01	—
V	0·03	2·9	<0·01	<0·01	25
Cr	0·49	1·8	<0·01	<0·01	—
Co	5·3	1·8	<0·01	<0·01	—
Ni	16	2·2	<0·01	<0·01	—

Analyses have been carried out on separated phases by inductively coupled plasma mass spectrometry. —, not determined.